Review Article **Open Access**

Yan Cheng, Ebuka S. Arinze, Nathan Palmquist, and Susanna M. Thon*

Advancing colloidal quantum dot photovoltaic technology

DOI: 10.1515/nanoph-2016-0017
Received September 10, 2015; accepted December 10, 2015

Abstract: Colloidal quantum dots (CQDs) are attractive materials for solar cells due to their low cost, ease of fabrication and spectral tunability. Progress in CQD photovoltaic technology over the past decade has resulted in power conversion efficiencies approaching 10%. In this review, we give an overview of this progress, and discuss limiting mechanisms and paths for future improvement in CQD solar cell technology. We briefly summarize nanoparticle synthesis and film processing methods and evaluate the optoelectronic properties of CQD films, including the crucial role that surface ligands play in materials performance. We give an overview of device architecture engineering in CQD solar cells. The compromise between carrier extraction and photon absorption in CQD photovoltaics is analyzed along with different strategies for overcoming this trade-off. We then focus on recent advances in absorption enhancement through innovative device design and the use of nanophotonics. Several light-trapping schemes, which have resulted in large increases in cell photocurrent, are described in detail. In particular, integrating plasmonic elements into CQD devices has emerged as a promising approach to enhance photon absorption through both near-field coupling and far-field scattering effects. We also discuss strategies for overcoming the single junction efficiency limits in CQD solar cells, including tandem architectures, multiple exciton generation and hybrid materials schemes. Finally, we offer a perspective on future directions for the field and the most promising paths for achieving higher device efficiencies.

Keywords: colloidal quantum dots, photovoltaics, solar cells, light trapping, optoelectronics

***Corresponding Author: Susanna M. Thon:** Department of Electrical and Computer Engineering, Johns Hopkins University, Baltimore, MD 21218, USA, E-mail: susanna.thon@jhu.edu
Yan Cheng, Ebuka S. Arinze: Department of Electrical and Computer Engineering, Johns Hopkins University, Baltimore, MD 21218, USA
Nathan Palmquist: Department of Materials Science and Engineering, Johns Hopkins University, Baltimore, MD 21218, USA

1 Introduction

Colloidal quantum dots (CQDs), semiconductor particles with dimensions on the nanometer scale stabilized in a solvent through anchoring ligands, have emerged in the last decades as a useful material in diverse applications such as light-emission [1–5], photodetection [6–9], biosensing [10–14] and photovoltaics [15–18].

This widespread interest stems from the desirable properties of CQDs including their solution-phase processing and spectral tuning via the quantum size effect, which in turn facilitates the manipulation of their optical and electrical properties. CQDs are a particularly promising solar cell material for several reasons. They offer the potential for the realization of low-cost devices [16, 19–22] through their ease of manufacturing [16, 23, 24], air stability [25–27] and film flexibility [28–35], thus making them compatible with roll-to-roll fabrication techniques. Though the true costs of scaling up CQD solar cell manufacturing to the gigawatt power scale are unknown, they are expected to be similar to those for organic photovoltaics [36] because of the similarities in materials, synthesis, and growth processes involved in the two technologies. Second, the steady rise in device efficiencies may indicate that CQD films combine the benefits of bulk semiconductors with those of solution-processed molecular materials [37–39]. Third, CQDs possess unique optical and electrical properties that could potentially be harnessed in strategies for overcoming the single junction Shockley–Queisser efficiency limit [40].

This last property is of particular interest for a number of advanced photovoltaic concepts. The band gap tunability of CQD materials creates a pathway through which tandem solar cells can be fabricated using a single materials system, thus eliminating the difficulty of finding a combination of materials with appropriate band gaps and suitable lattice matching for optimized multijunction cells [41–47]. Solution-based fabrication methods and infrared (IR) responsivity enable CQD films to be effectively combined with other materials in hybrid multijunction devices and serve as IR sensitizers. These properties also offer avenues for performance improvement via light

trapping and plasmonic enhancement techniques [48–53]. Lastly, CQDs may have the potential to overcome the Shockley–Queisser limit through multiple-exciton generation (MEG) [23, 54–59]. MEG can occur in semiconductors when a photon of energy greater than twice the band gap energy is absorbed, resulting in the generation of multiple charge carriers per single photon absorbed through impact ionization. MEG rates are predicted to be higher in CQDs than in traditional bulk semiconductors due to the discretization of the CQD energy spectrum [60, 61].

This review gives an overview of the field of CQD photovoltaics. We start with materials synthesis and fabrication methods and then discuss CQD optical and electrical properties of relevance for solar cell applications. Next, we outline the evolution and diversity of CQD solar cell device architectures. Lastly, we consider various advanced schemes for achieving high power conversion efficiency (PCE) in devices incorporating CQD materials and discuss the most promising avenues for the field moving forward.

2 Colloidal quantum dot synthesis and properties

2.1 Synthesis methods

The most common types of CQD materials used in solar cell applications are lead sulfide (PbS), lead selenide (PbSe), cadmium sulfide (CdS) and cadmium selenide (CdSe). PbS and PbSe possess small bulk band gaps, 0.41 and 0.27 eV, respectively [52, 62], making them ideal candidates for tuning the absorption spectra throughout the near-IR portion of the sun's spectrum. CdS and CdSe, with larger bulk band gaps of 2.42 and 1.74 eV, respectively, have found use in sensitized solar cell (SSC) architectures, and are of more interest for visible-wavelength applications [63, 64]. They have good absorption in the visible and UV spectrum, larger obtainable open-circuit voltage (V_{OC}) limits and have band edges well suited for coupling with many organic polymers.

A critical factor for most CQD device applications is the synthesis of highly monodisperse quantum dots. CQD size is controlled during synthesis by a number of factors, including temperature, precursor concentration and rate of conversion [54, 59] and degree of saturation. The synthesis of CQDs typically involves precursor decomposition forming monomers that undergo rapid nucleation followed by a slow growth phase [58, 65]. The synthesis reaction is initiated at a particular temperature, when the room temperature precursor is injected into a hot noncoordinating solvent (called the "hot injection method") [66]. The nucleation and growth processes are influenced by a number of factors including monomer concentration and reactivity, solution viscosity and reaction temperature.

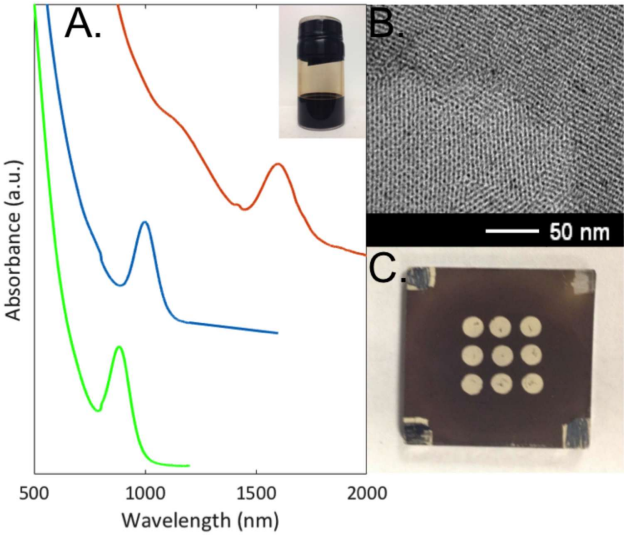

Fig. 1. (A) Solution-phase absorption spectra of PbS CQDs with excitonic peaks at wavelengths of 880, 1000 and 1600 nm. Spectra are offset for clarity. Inset: photograph of as-synthesized PbS CQD solution with excitonic peak at 955 nm. (B) Transmission electron microscope image of a large ensemble of PbS CQDs with excitonic peak wavelength of 950 nm. (C) Top-view photograph of a 3 × 3 array of PbS CQD photovoltaic cells (full substrate is 1 inch × 1 inch).

By varying the injection temperature, the size of the quantum dots can be tuned over a relatively large range [67]. Figure 1A shows absorption spectra for several PbS CQD solutions synthesized via the hot injection method with excitonic peaks in the range of 880–1600 nm, corresponding to CQD diameters of ~3–6.5 nm [68].

An alternative synthesis method, known as the "heating-up" method, involves mixing all precursors, reagents and solvent together at a low temperature and heating the mixture to a specific temperature [69]. This method yields similar size dispersity as the hot injection method, but may offer greater scalability potential due to its simplicity. Single-shot synthesis yields of up to 40 g of nanocrystals have been reported using this method [70]; typical syntheses utilizing the "hot injection" method yield about 0.5 g of nanocrystal material [70].

The most common precursors used for PbS and PbSe syntheses are lead oxide (PbO), oleic acid and *bis*(trimethylsilyl)sulfide ($(TMS)_2S$) or *bis*(trimethylsilyl)selenide ($(TMS)_2Se$) [58, 71]. However, $(TMS)_2S$ and $(TMS)_2Se$ are flammable and toxic, and they

readily hydrolyze with water to form toxic H_2S and H_2Se. This has led to the development of methods based on alternative precursors, including lead(II) chloride instead of PbO as the lead precursor to improve the surface passivation of the resulting CQDs [68, 72], and elemental sulfur instead of $(TMS)_2S$ [73, 74]. Additional novel growth methods have been proposed, including the synthesis of PbSe in a phosphate glass host [75]. The advantage of crystallizing QDs from the porous glass is that more homogeneous, larger crystal sizes exhibiting quantum confinement effects could be achieved versus those achieved in the conventional colloidal growth methods [76].

There are many other colloidal nanocrystal materials that have been synthesized using variations of these methods, including single element materials, such as graphene [77], silicon and germanium, and compound materials. These compounds include binary, mostly III–V and II–VI semiconductors such as metal chalcogenides [78–80], as well as ternary and quaternary compounds [81–84].

2.2 Ligand types

Ligands play an important role in CQD synthesis and electronic film properties [85]. Their main function is to maintain colloidal stability in the solution phase and prevent CQDs from aggregating during the nucleation stage of synthesis. Pb- and Cd-chalcogenide CQDs as-synthesized typically have Pb- and Cd-rich surfaces [27, 86–88]. There, the ligands also play an important role in passivating electronic trap states that are otherwise present due to the presence of undercoordinated surface atoms. Additionally, ligands help to protect CQDs from oxidative degradation, and can facilitate electronic coupling between neighboring CQDs in the film phase. Long organic ligands, however, can act as electronic tunneling barriers, where the rate of charge transport through the barrier decreases exponentially with the barrier width and the square root of the barrier height [89–92].

Ligand selection can therefore have a large impact on CQD solar cell performance, and much effort has been directed in the field toward engineering ligands for better device operation. Popular ligands for CQD electronic film applications include alkane and aromatic thiols, amines and carboxylic acids [16, 85, 93–96], metal chalcogenide complexes [90] and halogen atoms [97]. Most organic ligands consist of three parts: an inner anchor to the quantum dot, a middle hydrophilic segment and an outer functional group. The freedom in choosing a functional group gives ligated CQD materials versatility for different applications.

Metal chalcogenides and metal halides are alternatives to organic ligands commonly used for CQDs in solar cells. Treatment with metal chalcogenide complexes, such as $In_2Se_4^{2-}$ [98, 99], $\{In_2Cu_2Se_4S_3\}^{3-}$ [98] and $Sn_2S_6^{4-}$ [90], has been shown to improve interparticle coupling over the use of organic ligands [90] in CQD thin-film field-effect transistors.

Metal halide ligands are well suited for trap state passivation, as their small size allows them to access and passivate exposed surface sites inaccessible to longer organic ligands. Studies have shown that device air stability and efficiency are greatly increased when the CQD active material is treated with Cl-containing ligands [16, 72]. Several specific methods have been developed that take advantage of the properties of halogen ligands. These include a PbS CQD treatment procedure that deployed iodine-based materials to create an air-stable ink [100], and a PbS/CdS core-shell CQD synthesis method that used chlorine-based ligands to achieve a V_{OC} of 0.66 V through the large band gap of CdS and the passivating effects of the Cl [101]. The highest performing CQD solar cells today incorporate some halide-based ligands into their CQD films [23, 102].

2.3 Film processing

The most prevalent method of forming CQD films for solar cell applications involves layer-by-layer deposition. This process can be carried out under inert or ambient conditions and involves several deposition iterations, as the name implies. One processing step typically includes deposition of the CQDs, followed by a solid-state ligand exchange that densifies the film rendering it insoluble, and several washes with an organic solvent to remove the exchanged ligands [103, 104]. The ligand exchange process is vital to improve the overall conductivity of the thin film, as it replaces the long aliphatic synthesis ligands with shorter, often bifunctional, linkers [105].

Methods for depositing the CQDs vary, and include spin-casting [6, 17, 18, 41], dip-coating [106, 107], drop-casting [108,109], spray-coating [110–113] and doctor-blading [114, 115]. Figure 1C shows a CQD solar cell array in which the PbS CQD film was spin-cast using a layer-by-layer deposition process to build up a thick film.

One drawback of the layer-by-layer process is the inefficient use of materials inherent in spin-casting, dip-coating and spray-coating processes. Several methods have been proposed to address this limitation, such as developing nanoparticle inks using solution-phase exchanges to shorter ligands [116]. This process allows deposition to occur in a single step that utilizes nearly 100% of

the CQD starting solution, and offers distinct material and scalability advantages over the layer-by-layer method.

2.4 Optical properties

The optical properties of CQDs are determined by the size, composition, ligand structure and shape of the individual quantum dots [55, 56, 117–119]. The size of the CQD has a direct impact on the apparent band gap, with smaller quantum dots exhibiting higher excitation energies. This is quantitatively shown via the Brus equation [120]:

$$E^{\star} = E_g + \frac{h^2\pi^2}{2R^2}\left[\frac{1}{m_e} + \frac{1}{m_h}\right] - \frac{1.8e^2}{\epsilon_o\epsilon_p R} \quad (1)$$

Here, $E^{\star}$ is the apparent band gap, E_g is the bulk band gap, m_e and m_h are the respective effective electron and hole masses, ε_p is the dielectric constant of the nanoparticle and R is the nanoparticle radius. This formula includes the additive component of the quantum confinement of the excitons as well as the subtractive component of the electron-hole repulsion. For PbS CQDs, a prevalent material for CQD solar cells due to its optimal band gap tuning range, Moreels *et al.* showed that the following empirical equation is a good approximation of the relationship between the effective band gap (in eV) of the CQD and its diameter, d (nm) [121]:

$$E^{\star} = 0.41 + (0.0252d^2 + 0.283d)^{-1} \quad (2)$$

Particle size influences optical properties beyond tuning the absorption onset. The ambient stability of PbS CQDs has also been demonstrated to be dependent on the nanoparticle size [57]. The excitonic wavelength of larger CQDs (diameter >4 nm) experiences a blue shift when stored in air, as the un-passivated (100) surface becomes oxidized and the effective optical particle diameter decreases [57]. It was also shown that the molar extinction coefficient increases with the CQD volume as d^3 (where d is particle diameter) at higher energies, but only increases as $d^{1.3}$ near the band gap [121].

Electroluminescence efficiency is viewed as a good indirect measure of the open-circuit voltage of a solar cell; thus, achieving large luminescence yields is a requirement in photovoltaic materials. At open-circuit, high luminescence efficiency implies the absence of nonradiative sources of recombination in a solar cell [122]. Typical as-synthesized CQD solutions possess photoluminescence quantum efficiencies (PLQE) around 50%, and treatments such as a cadmium chloride ($CdCl_2$) metal-halide passivation strategy have been shown to help CQD solutions maintain these efficiencies even after the washing steps necessary to prepare the CQDs for film deposition [17]. Film-phase PLQEs are much lower, substantiating the view that CQD film transport is limited by nonradiative recombination processes induced by the large electronic trap state densities.

Additionally, emission in CQDs is red-shifted with respect to the first (1S) excitonic absorption peak [123]. This difference between the luminescence energy and the absorption energy is referred to as the Stokes shift, and it decreases with increasing quantum dot size. The relatively large Stokes shifts observed in CQDs have been partially attributed to the surface properties of the nanoparticles [124].

Ligands play an important role in the optical properties of CQDs. Better passivated surfaces can increase radiative recombination efficiency, leading to higher photoluminescence quantum yields. Ligands can also facilitate coupling between quantum dots, which can have the effect of red-shifting the absorption and emission spectra and increasing exciton dissociation rates, thereby lowering radiative recombination rates. One study showed that photoluminescence quantum yields could be increased by a factor of 2 when using glutathione (GSH) over tiopronin ligands due to the presence of an inner thiol group in the GSH ligand [125]. Silva *et al.* later showed that the partial hydrolysis of GSH caused some of the sulfur to react with the CdTe to create a CdS shell that provided better surface passivation [126]. Another study found that when comparing bifunctional carboxylic acid molecules, the more acidic and shorter chains performed the best optically, leading to an excitonic absorption peak red shift due to greater electronic coupling between neighboring dots [127]. This electronic coupling, also seen in the study of 1,3-benzenedithiol (1,3-BDT), ethanedithiol (EDT), mercaptopropionic acid (MPA) and ammonium sulfide, was attributed to the extension of the electron wave function outside the individual CQDs [128]. This resulted in a reduction of the quantum confinement of the particles, decreasing the apparent band gap of the CQDs.

MEG is a potentially useful phenomenon that is predicted to occur at higher efficiencies in quantum-confined nanostructures compared with bulk semiconductors [129, 130]. MEG can occur when a photon with energy greater than twice the band gap energy is absorbed. This effect is explained by impact ionization, during which a high energy, excited carrier decays by transferring its energy to the promotion of additional electron-hole pairs [131]. Harnessing MEG in a solar cell device could lead to improved photovoltaic conversion efficiency, as it increases the generated photocurrent while simultaneously restricting heat generation resulting from phonon scattering [60]. MEG has

been measured in studies involving both solution-phase and thin-film CQD materials [60, 61, 132].

2.5 Electronic properties

Critical electronic film parameters that influence CQD solar cell performance include carrier mobility, trap density and diffusion length (Table 1). Carrier mobility refers to the speed at which holes or electrons move under an electric field. Typical carrier mobilities in CQD solar cell films have been measured in the range of 10^{-4} to 10^{-2} cm^2/Vs [94, 133, 134]. Carrier mobilities as high as 8×10^{-2} cm^2/Vs have been observed in recent PbS CQD photovoltaic film studies [134].

Electronic states that lie within the band gap of a semiconductor are referred to as trap states, and their density is usually reported as a measure of material purity. They are detrimental to photovoltaic device performance, as they act as recombination centers for charge carriers. Trap states within CQD films have a variety of physical origins; they can exist on the surface of CQDs due to incomplete surface ligand coverage, and larger-than-average CQDs can also introduce electronic states within the band gap of a CQD film. Trap state densities in PbS CQD solar cell films have been reported in the 10^{16}–10^{17} cm^{-3} eV^{-1} range [17, 133, 135, 136]. Studies have found that trap state densities in CQD films are sensitive to air [136]. After leaving a EDT-treated PbS CQD film exposed to air for 2 days, the trap state density increased sixfold from 2.7×10^{16} to 1.8×10^{17} cm^{-3} eV^{-1} [136]. This was likely due to the exposure of the films to oxygen and water, which shifted the Fermi level and lowered the measured short-circuit current (J_{SC}) by 23%. A recent study identified adsorbed oxygen molecules as the mostly likely origin of in-gap states measured to lie ~200 MeV above the valence band edge in a PbS CQD film [137].

Diffusive transport has been a limiting factor in CQD solar cell performance. Typical diffusion lengths in CQD photovoltaic films have been measured to be in the range of 50–100 nm [120, 138]. A recent study demonstrated a record diffusion length of 230±20 nm by tuning the ligand structure to enable partial fusing of the CQDs without sacrificing their overall optical properties [134]. Table 1 contains a summary of the mobilities, trap densities and diffusion lengths measured in several PbS CQD photovoltaic device studies.

2.6 CQD solar cell devices

CQDs can be deployed in multiple solar cell device architectures. CQD thin films display semiconducting behavior, and device designs based on these materials have taken inspiration from bulk semiconductor cells and organic solar cells. Additionally, CQDs have been used as a sensitizing material in electrochemical solar cell designs. Improvements in CQD solar cell efficiencies have relied on both materials development and device architecture engineering. This section gives a brief introduction to solar cell operation and overviews the progress in CQD solar cell device designs and performance.

Solar cells are two-terminal optoelectronic devices that convert light into electricity via the photovoltaic effect. Their operation is typically quantified by several figures of merit, which we will use in the following section. The short-circuit current, I_{SC}, is the current that flows through a photovoltaic device at zero bias. I_{SC} depends on the generation and collection of charge carriers, and the area-independent short-circuit current density, or J_{SC}, is often employed in its place. The open-circuit voltage, V_{OC}, is the maximum photovoltage obtained from a solar cell device at zero current. The V_{OC} is largely dependent on the band gap or absorption edge of the photovoltaic material and can be reduced by recombination processes. The fill factor, FF, is a measure of the squareness of the current-voltage curve and is defined as the ratio of the current times the voltage at the device maximum power point of operation to $I_{SC} \times V_{OC}$. The PCE is the ratio of the maximum power from the device to the input power from the sun, and is usually calculated as $J_{SC} \times V_{OC} \times FF/100$ mW/cm^2, where 100 mW/cm^2 is the AM1.5G standard terrestrial solar irradiance.

2.7 Hybrid polymer-CQD and Schottky CQD photovoltaics

Early devices that used CQDs as the absorbing layer employed a Schottky or metal-semiconductor junction for operation [52]. They relied primarily on the difference in work functions for the transparent conductive oxide (TCO), and the top metal electrode to generate a built-in field and promote the flow of a photocurrent across the absorbing medium. This absorbing medium was initially a polymer-CQD composite layer; however, after further studies on the electronic impact of the polymer [139], the composite was replaced with a pure CQD layer. Figure 2A shows the structure of a CQD Schottky junction solar cell.

Table 1. Summary of electronic properties measured in PbS CQD solar cell films employing different ligand strategies.

Material	Carrier mobility (cm^2/Vs)	Trap density ($cm^{-3}\ eV^{-1}$)	Diffusion length (nm)
Untreated [17, 94, 135]	$<1 \times 10^{-4}$ (hole)	1×10^{17}	<10
MPA-treated [133, 135]	5.1×10^{-3} (electron)	2×10^{16} to 5.4×10^{16}	40±10
EDT-treated [94, 133]	1×10^{-4} (hole) 2.4×10^{-4} (electron)	8×10^{16}	
$CdCl_2$-treated, MPA-treated [17, 134, 135]	4.2×10^{-3} (hole) 2.1×10^{-2} (electron)	1.8×10^{16}	60±10
RnH_2-Cl-passivated, $CdCl_2$-treated [134]	8×10^{-2} (electron)		230±20

These solar cell designs that used CQDs as both the absorbing medium and charge transport medium were based on the rectifying junction present at the p-type PbX (X = S or Se) CQD film and shallow work function metal interface. Various materials, including Al, Ca, Mg and Ag have been used as the shallow work function metal in Schottky devices [18, 107, 140, 141]. Improvements in the performances of these devices led to PCEs exceeding 3%, and air stability was improved through engineering of the stabilizing ligands [142]. The air stability was further improved through the insertion of a LiF blocker at the semiconductor–metal interface to limit degradation [143]. Further studies on improving the air stabilities of Schottky cells have involved inverting the junction [144] and oxidation of the CQDs at the semiconductor–metal interface [145].

The CQD Schottky architecture has several advantages, such as functional simplicity and ease of fabrication, and has achieved PCEs exceeding 5% [146]. The major drawback of this architecture is Fermi level pinning at the rectifying junction which limits the V_{OC} to well under the band gap of the material [147, 148].

2.8 CQD-sensitized photovoltaics

The IR sensitivity and high absorptivity of CQDs makes them attractive materials for use as sensitizers in electrochemical solar cell architectures [149–151].

In these SSC devices, a monolayer of CQDs coats a porous electron acceptor (usually titanium dioxide [TiO_2] or zinc oxide [ZnO]), and hole transport and extraction is provided by an infiltrated electrolyte. Compared with traditional dyes, CQDs are appealing due to their band gap tunability via the quantum size effect [152], large intrinsic dipole moment for efficient charge separation [153–155], potential for efficient MEG by impact ionization [60, 61, 130] and relative stability under illumination [156–158]. Figure 2B shows the architecture of a photovoltaic cell employing CQDs as sensitizers.

An observed issue in CQD-SSC devices is the detrimental presence of high shunt resistance. In addition, the small average size of the electron acceptor pore openings makes obtaining a continuous monolayer of infiltrated CQDs difficult to achieve. Studies have shown that at saturation, only 14% of the real electron acceptor surface area is covered by CQDs [159]. This leads to the presence of shorts at the locations deficient of CQDs, due to the direct contact between the two charge transporting media. Performing ligand exchanges, where the original lengthy ligands are substituted for shorter bifunctional ligands, has improved CQD loading due to the enhanced anchoring of CQDs to the titania electrode [160, 161]. Alternative loading methods, including a pressing technique [162] and electrophoretic deposition [163], have led to improved CQD loading and elimination of regions exposed to the redox electrolyte. In recent studies, pH control was demonstrated to increase quantum dot loading as well as reduce interfacial recombination in CQD-SSC devices [164, 165].

Although performances continue to rise in these device architectures, efficient deposition of high-performing presynthesized CQDs into the nanoporous electrodes is a challenge. Alternative loading methods have included using chemical bath deposition (CBD) [166–168], successive ionic layer adsorption and reaction (SILAR) [161, 169, 170] and ion layer gas adsorption and reaction to form CQDs *in situ* [171]. A recent study has shown that although the SILAR loading method provides more intimate interfacial contact, resulting in efficient charge injection and higher photocurrents, sensitization using *ex situ* synthesized CQDs leads to longer electron lifetimes [172].

PCE improvement for these architectures focuses on three main schemes: (1) FF enhancement, by integrating counter electrodes that are compatible with polysulfide electrolytes [173–176], (2) short-circuit current enhancement, by improving absorption in the CQD materials or harvesting the near-IR portion of the spectrum [156, 177] and (3) open-circuit voltage enhancement, through the use of alternative redox systems or by suppressing interfacial recombination [178, 179]. The highest PCE to date achieved in a CQD-SSC device is 8.21% [180]. In this study, a novel sequential double-layer treatment on the CQD-sensitized photoanode was demonstrated to suppress interfacial recombination while enhancing cell stability.

2.9 Depleted heterojunction CQD photovoltaics

As a means to overcome the limitations of the Schottky junction architecture, as well as to combine the merits of the Schottky and CQD-SSC architectures, the depleted heterojunction (DH) CQD solar cell was developed [181]. The DH architecture consists of an n-type electron acceptor forming a heterojunction with a p-type CQD film [181]. The full device structure starts with a substrate (usually glass or a flexible transparent material) with a transparent conductive oxide (usually indium tin oxide or fluorine-doped tin oxide). The electron acceptor or n-doped layer is a wide band gap semiconductor, such as TiO_2 or ZnO, and the absorbing p-type CQD film layer is deposited on top of this layer. Finally, the device is completed with an optional highly doped metal oxide, such as molybdenum trioxide (MoO_3), and a hole-collecting deep work function metal such as gold. Figure 2C shows the architecture of a photovoltaic cell employing the DH design.

An additional limitation of Schottky junction devices is the distance between the photogeneration plane, located near the CQD-TCO interface, and the charge separation junction, located at the CQD–metal interface. The DH architecture eliminates this issue as photogeneration occurs very close to the metal oxide–CQD junction itself. The doping levels of each material determine the depletion widths on both sides of the junction; typically, the n-type wide band gap semiconductor is highly doped to ensure that more of the depletion region falls on the CQD film side. The electric field associated with the depletion layer helps promote charge extraction through the CQD film by extending charge transport beyond the carrier diffusion length [182].

Several improvements in the performance of DH devices have been made as a result of materials development and architectural modifications. Improvements in the band alignment between the CQD layer and the wide band gap semiconductor have been made to ensure efficient injection of electrons [23]. Depletion widths have been extended through the use of p-i-n architectures, resulting in improved charge extraction and increased absorption [183]. Band alignment and doping engineering in CQD solar cells will be discussed in depth in a later section.

Many CQD solar cell performance advances have relied on ligand engineering. Most high-performing devices utilize short thiol ligands [184] in combination with inorganic halide ligands [16], which are delivered through solid-state or solution-phase ligand exchanges. Improved ligand strategies typically lower the density of mid-gap electronic trap states while increasing diffusion lengths and carrier mobilities [16, 95, 134, 135, 185].

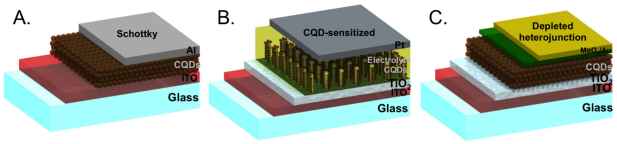

Fig. 2. Schematics of different CQD solar cell architectures employing: (A) a Schottky junction, (B) CQDs as sensitizers, (C) a depleted heterojunction.

The highest certified PCE to date of 9.9% has been achieved in a modified DH architecture [102]. Despite ongoing advances in CQD solar cell efficiencies, performance is still limited by short charge carrier transport lengths in CQD films. The discrepancy between the relatively long IR photon absorption lengths in CQD materials and the smaller charge carrier transport lengths is referred to as the "absorption-extraction compromise". The absorption lengths in CQD films are typically near 1 μm at the optimum single junction IR band gap wavelengths [186]. As summarized in Table 1, maximum diffusion lengths of about 230 nm have been achieved in CQD films using RnH_2-Cl or $CdCl_2$ passivation, leaving a discrepancy of a few hundred nanometers between the absorption and transport length scales. The maximum photocurrent possible for a material with a band gap of 1.3 eV is calculated to be 36 mA/cm^2 [148]; maximum photocurrents achieved in CQD SCs with band gaps near 1.3 eV today are approaching 30 mA/cm^2 [23, 25, 187, 188]. Therefore, photocurrent enhancements on the order of at least 20% are needed to approach the theoretical limits.

Methods to overcome this limitation include materials engineering [96, 189–191], device architectural modifications [192–196], incorporation of light trapping techniques to decrease the effective film absorption lengths [197–202] and the integration of plasmonic elements to enhance absorption in the CQD material [203–208]. These strategies, along with other advanced techniques, will be discussed in the following sections.

3 Advanced CQD solar cell concepts

3.1 Device architectures for enhancing carrier extraction

3.1.1 Bulk heterojunctions

Although heterojunction CQD photovoltaic devices have achieved higher open-circuit voltages and FFs compared with Schottky devices, the performance is still constrained by short carrier diffusion lengths. A large fraction of the generated carriers do not contribute to the extracted photocurrent in these devices but, instead, are lost through nonradiative recombination processes. Similar compromises between absorption and charge extraction have been observed in other solar cell materials. Bulk heterojunction (BH) device designs, in which donor and acceptor phases are mixed together to increase the charge-separating interfacial area, have been used successfully in organic solar cells. These device structures enable enhanced exciton dissociation while allowing the thicknesses of the absorbing layers to be increased.

Taking inspiration from this concept, depleted BH devices were developed for CQD solar cells. A porous TiO_2 layer infiltrated with PbS CQDs was developed to form a CQD depleted BH [15]. This design effectively increased absorption, especially in the IR near the band gap energy, and improved carrier collection efficiency by facilitating more complete depletion of the CQD film. The increase in bimolecular recombination due to the large interfacial area was ameliorated by the induced electric field and a titanium chloride treatment, which effectively passivated the TiO_2 matrix.

Additional advances in BH structures included the use of nanowires to increase the CQD film loading fraction [209, 210]. Figure 3 illustrates a bottom-up fabrication technique that was used to realize nanowire network TiO_2 electrodes for a CQD BH solar cell. Dense ZnO nanowires were first synthesized by a hydrothermal method. Subsequently, TiO_2 nanowires were formed by a liquid-phase deposition (LPD) process while the ZnO was etched away by the HF, which formed during the process. The final nanowire fabrication step was a titanium tetrachloride ($TiCl_4$) treatment to fill in the porous nanowire surfaces. PbS CQDs were infiltrated into the nanowire network. The extension of the depletion region within the absorbing material allowed for the incorporation of thicker CQD films. This led to absorption enhancements, particularly in the IR region of the spectrum, and higher external quantum efficiency (EQE), indicating that high collection efficiency was maintained in the thicker devices. Short-circuit densities were increased from 19.8 mA/cm^2 in planar control devices to 22.5 mA/cm^2 in the best performing nanowire devices.

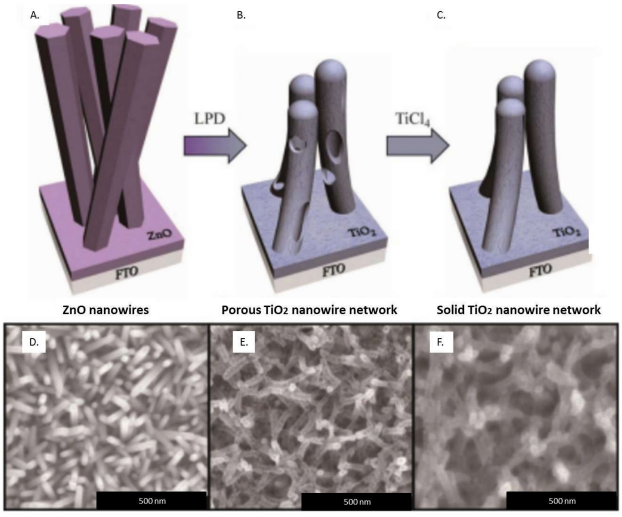

Fig. 3. Fabrication procedure for TiO_2 nanowire network electrodes for CQD BH solar cells. (A, D) ZnO nanowires were first synthesized on an FTO substrate via a hydrothermal method. (B, E) The ZnO nanowires were converted to porous TiO_2 nanowire networks via LPD. (C, F) Solid TiO_2 nanowire networks were formed as a result of $TiCl_4$ treatment. Reprinted with permission from [209]. Copyright 2013 Wiley-VCH Verlag GmbH & Co. KGaA.

ZnO nanowires fabricated using the same method have also been used directly as the electrodes in a BH CQD solar cell [211]. After optimization of the nanowire size, devices exhibited short-circuit current increases of 50% over planar controls, leading to 35% increases in PCE. The study revealed that the ordering and uniformity of the nanowires strongly affected the carrier transport, with nonuniform nanowires acting as additional sources of series and shunt resistance in the cell. Insertion of a MoO_3 interlayer between the ZnO nanowire-CQD film composite and the back electrode was necessary to prevent device shorting.

A device design with similar inspiration is the bulk nano-heterojunction (BNH), in which the active layer is made of mixed phases of n- and p-type nanoparticles. One demonstration consisted of a blend of p-type PbS CQDs and n-type Bi_2S_3 nanoparticles [212]. The measured carrier lifetime in a cell with an optimized blend ratio of PbS and Bi_2S_3 materials was three times longer than in the bilayer control device. The improved absorption, carrier transport, and carrier collection led to a threefold short-circuit current enhancement and a PCE of 4.87%.

Further improvements in the BNH design relied on the formation of pathways for better carrier transport by introducing hyperbranch-shaped CdSe nanoparticles [213]. Compared with isolated CdSe quantum dots, these nanoparticles formed a continuous network, which theoretically provided an efficient transport channel for electrons and holes. The improved carrier collection contributed to a dramatic improvement in cell performance and a PCE of 5.72%.

3.1.2 Graded doping device designs

Other strategies to increase charge extraction focus on enhancing the built-in field or increasing the depletion width within the CQD film by modifying the doping densities of the various cell layers. A p-i-n device architecture accomplishes this goal [183]. Studies employing p-i-n CQD device designs aim to increase absorption by including thick intrinsic CQD layers sandwiched between highly-doped n-type metal oxides and p-type CQDs treated with alternative ligands. These designs have led to improvements in short-circuit current and open-circuit voltage. Overall performance has been limited by low FFs due to the large series resistance of the thick intrinsic layer, ultimately leading to PCEs of 3.4% [214].

Another graded doping study used a p^+ PbS/n PbS/n^+ PbS design in a quantum junction (QJ) cell [215] that improved carrier extraction by introducing a electric field through the doping gradient. Bromide and iodide-based ligands were used to realize lightly and heavily doped n-type PbS in the structure. Efficient charge separation was enabled by the separation of the Fermi-levels through the high doping densities, resulting in both higher V_{OC} and FF compared with a conventional QJ reference cell.

Graded doping schemes have also been implemented in DH cells. One study used both p and p^+ PbS layers in a PbS/TiO_2 solar cell [216], where the order-of-magnitude difference in doping densities was achieved through 3-mercaptobutyric acid and 3-mercaptopropionic acid ligand strategies, respectively. At the maximum power point, the graded doping devices maintained high photocurrent close to the J_{SC} value due to their superior carrier extraction efficiency. V_{OC} was slightly degraded due to the suppression of the quasi-Fermi level splitting.

3.1.3 Band engineering in CQD solar cells

To date, the best open-circuit voltages demonstrated in CQD solar cells are still significantly below the theoretical limits based on the band gap of the materials. Bulk recombination in the CQD layers, at interfaces and in metal oxide electrodes, as well as Fermi level pinning are sources of the low V_{OC}. Band engineering of the device layers is one potential method for achieving higher V_{OC} values in CQD solar cells.

The n-type metal oxide electrodes can be engineered to reduce cell voltage losses. In ZnO, a long conduction band tail of states is frequently observed. These band gap states are detrimental to carrier extraction since they contribute to electron trapping and loss at interfaces, leading to a lower V_{OC}. This issue can be alleviated by doping ZnO with Mg [217]. With increased doping concentrations, the conduction band edge of ZnO was raised to reduce the density of states below the PbSe CQD film conduction band edge in one solar cell demonstration [217].

Interface defects are present in both Schottky and heterojunction CQD solar cell devices, leading to fast recombination rates and carrier loss. Air annealing at mild temperatures and UV/ozone treatments have been used to form a thin oxide layer within the PbS CQD film in a Schottky junction device [145]. This resulted in the removal of some interface states and introduced a larger amount of band bending to the cell. The result was higher V_{OC} and FF compared with a nonoxidized cell.

Interface recombination can be especially severe in BH architectures since the interfacial area is large compared with planar devices. A ZnO nanowire passivation scheme using a thin TiO_2 surface layer prepared by CBD [218] resulted in significant trap state reduction in one study and improvement of solar cell V_{OC} from 0.3 to 0.42 V. However, addition of oxide layers can also increase the cell series resistance and therefore must be carefully designed to achieve a net performance benefit.

Introducing buffer layers into CQD solar cells can also be used as a band engineering tool and can reduce carrier loss at interfaces [219–221]. Organic materials are good buffer candidates as they exhibit low trap state densities. One demonstration used a [6,6]-phenyl-C61-butyric acid methylester (PCBM) buffer layer in a CQD heterojunction solar cell which resulted in long carrier lifetimes, leading to 20% PCE enhancement over a control device without the buffer layer [220].

Another promising strategy involves modifying the interfacial band structure itself to suppress recombination processes. The piezoelectric effect can be used to induce polarization at a CQD heterojunction interface. In practice, this has been achieved by using compressively strained ZnO to induce a positive piezoelectric field polarization [222]. By changing the interfacial charge distribution, the depletion width was extended within the CQD

film, and a larger band offset was realized, leading to improved carrier generation and extraction. This method decreases in effectiveness with higher illumination intensities due to the polarization screening effect.

Deep work function metals such as gold are used to form Ohmic contacts to p-type CQD films. However, Schottky barriers can form at the CQD–metal interfaces due to Fermi level pinning. Thus, MoO_3 is often used to pin the Fermi level on the electrode to avoid forming a Schottky junction and facilitate efficient hole collection [223].

Ligand treatments have also been demonstrated as an effective method for engineering band alignments. One study showed that the conduction and valence band energy levels of similarly sized PbS CQDs can shift by up to 0.9 eV due to different ligand treatments [224]. In another study, high power conversion efficiencies (8.55%) as well as superior air stabilities were achieved through the application of different ligand treatments, effectively engineering the relative band alignment at the CQD interfaces with the selective electrodes [23]. Eliminating the MoO_3 layer, as well as using inorganic ligand-passivated CQDs as the absorbing layer, was found to be crucial in obtaining ambient stability.

Using core-shell quantum dots has also been proposed as a mechanism to decrease trap-state densities associated with CQD surface defects and improve device stability. PbSe/PbS [214] and PbS/CdS [225] core-shell quantum dots have been reported to facilitate higher conductivity and efficient carrier injection into TiO_2. Using band alignment engineering between the core and shell materials for optimal separation of electrons and holes led to a PCE of 3.93% in a device employing core-shell CQDs [163].

3.1.4 Quantum funnels

The quantum funnel device is another concept developed to enhance carrier transport in CQD photovoltaics. It takes advantage of the size-tuning effect of CQDs to layer semiconductors with different band gaps and create a photoelectron potential "funnel" [45]. This potential cascade design induces an additional built-in electric field and serves as a driving force, which improves the minority carrier transport in device demonstrations. Longer wavelength photons were absorbed closer to the junction, which increased the FF of a graded solar cell [39]. A subsequent study demonstrated efficient exciton transfer mechanisms in EDT- and 1,3-BDT-treated funnels, resulting in enhanced carrier transport and photocurrent [226]. Centrifugal casting has also been employed as a one-step deposition technique to form CQD films with a graded band gap structure from a mixture of different sized CQDs, which greatly simplified the quantum funnel fabrication process [227].

3.1.5 Quantum junction devices

In theory, homojunction-type devices offer advantages over heterojunction devices due to the elimination of potential voltage losses due to band offsets. Fabricating such a structure out of CQD films has been difficult due to the need to engineer both n- and p-type behavior in these materials. An initial QJ demonstration was enabled by the fabrication of stable n-type CQD films [46].

The doping character of CQD films is determined by the net stoichiometry of the system considering both the CQD cores and ligands. In practice, CQD doping types are affected by the ligands and the chemical processing environments. Halide anion ligands, delivered through tetrabutylammonium iodide or cadmium bromide/iodide treatments, have proven to be efficient in achieving n-type doping of CQD films under inert atmosphere processing conditions [25, 228]. Additionally, PbS CQDs can be treated with Ag ions during synthesis to increase the doping density on the p-side of the junction, thereby extending the electric field farther into the lightly doped n-type films [229]. Bi-doping has also been successfully used to achieve n-type doping of PbS CQDs [230].

Further optimization of the QJ device design resulted in a field-enhanced device, which employed engineering of the electric field profile of the junction region [231] as shown in Figure 4. Slightly smaller nanoparticles were employed on top of the main absorbing CQD layer, which led to both higher open-circuit voltage and short-circuit current in the field-enhanced solar cell.

3.1.6 Light trapping in CQD solar cells

The small charge transport lengths in CQD films limit the thickness of the active layers that can be used in solar cells. This has a negative effect on device absorption, especially at longer IR wavelengths. Light trapping, where effective photon absorption lengths are increased via structuring of the device layers, is a potential method to overcome this limitation. Incorporating structured electrodes to form BH devices is a strategy that can be extended to light trapping. In addition to enhancing carrier extraction, structured electrodes can serve as optical scatterers and in-couplers to enhance photon absorption.

One study used polystyrene microspheres to introduce nanoscale pores with diameters of about 300 nm into the

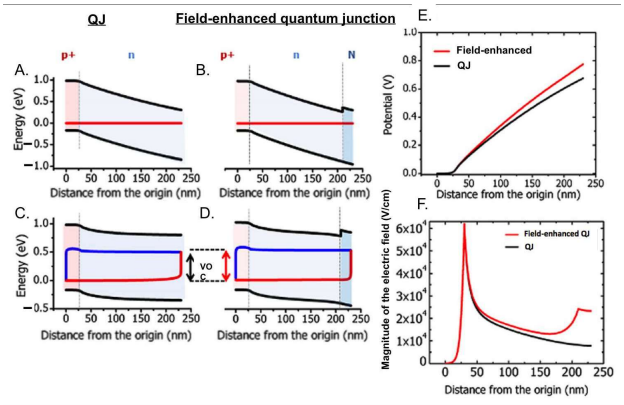

Fig. 4. (A, B) Simulated equilibrium band diagrams of QJ and field-enhanced QJ structures, respectively. (C, D) Simulated band diagrams at open-circuit conditions for the same structures as in (A) and (B), respectively, under 1000 W/m^2 solar illumination. The field-enhanced QJ design exhibits a higher open-circuit voltage due to the increased separation between the Fermi levels of the p- and n-type layers and (E) a higher built-in voltage at equilibrium. (F) Simulated electric field inside the solar cell active layers at the maximum power point. The field-enhanced QJ architecture exhibits a higher electric field magnitude. The electric field vector is directed toward the p-layer, driving minority holes toward their selective contact during photovoltaic operation. Reprinted with permission from [231]. Copyright 2013 AIP Publishing LLC.

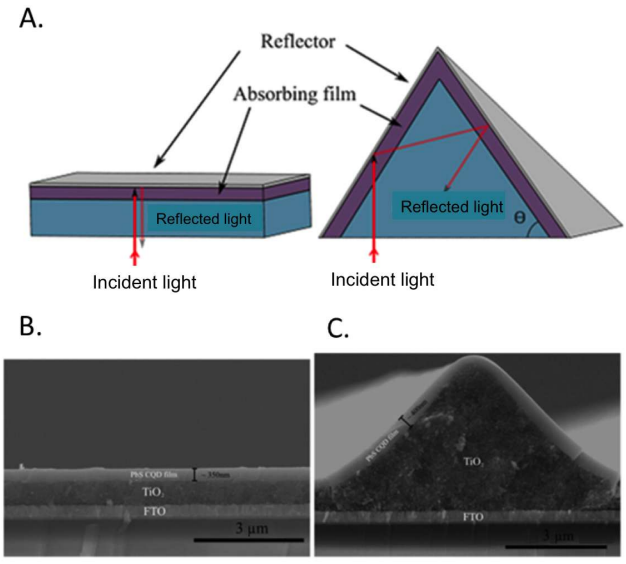

Fig. 5. (A) Schematics of planar (left) a pyramid-patterned (right) thin-film solar cells, illustrating the increased light-path-length advantage of pyramid-patterned electrodes. (B) Cross-sectional scanning electron microscope image of a planar CQD device. The film thickness is ∼350 ±30 nm. (C) Cross-sectional scanning electron microscope image of a pyramid-patterned CQD device. The film thickness is ∼400 ±30 nm. Reprinted with permission from [233]. Copyright 2015 American Chemical Society.

TiO_2 electrode [232]. The size of the pores led to absorption enhancement in the CQD films due to scattering from the electrode at visible and near-IR wavelengths. The EQE enhancement over a wavelength range of 400–1200 nm also included contributions from improved carrier transport due to the BH structure.

Another study used a stamping process to fabricate micron-scale pyramid-shaped TiO_2 electrodes in combination with conformal CQD deposition [233]. A schematic of the structure and light path in both planar and pyramid-shaped devices is shown in Figure 5. The pyramid shape was demonstrated both theoretically and experimentally to be beneficial for increasing the optical path lengths within the active material at wavelengths longer than 600 nm. Compared with planar devices, the hierarchically structured CQD solar cells achieved a short-circuit current density enhancement of 24% and a maximum PCE of 9.2% with negligible effect on the open-circuit voltage and FF. The pyramid angle of 54.7 degrees was chosen due to silicon's natural etch plane for ease of fabrication; sharper pyramid angles of up to 80 degrees were predicted to result in even larger absorption enhancements, but would require advanced fabrication techniques.

Another study used a soft nano-imprinting technique to pattern a diffraction grating into an indium tin oxide (ITO) electrode and increase absorption near the excitonic peak wavelength of the PbS CQDs in a solar cell [234]. The fabrication process used an epoxy stamp, which was left as part of the device to reduce the number of processing steps. Spin-cast ZnO was deposited on top of the ITO grating, and a PbS CQD layer planarized the device. In comparison to the flat device, solar cells with the imprinted electrodes exhibited a onefold increase in light absorption from 600 to 1100 nm in wavelength. The enhanced absorption directly contributed to the 17.5% increase in device photocurrent while maintaining similar FF and open-circuit voltage as in the planar devices.

Nanophotonic light trapping schemes have also been used in CQD solar cells. A periodic structured PbS CQD solar cell (Figure 6) was fabricated using nanosphere lithography to create nanopillars in the glass substrate with rationally designed geometrical features [235]. In this architecture, the nanostructure was propagated from the substrate through the device layers using conformal coating processes. At the interface between the top Au electrode and the PbS CQD film, a significant increase in field intensity was predicted to occur using finite-difference time-domain simulations. This increase was ascribed to surface plasmon polaritons excited in the structured Au electrode. Furthermore, this structure also demonstrated less reflection in comparison to planar devices. The absorption

thus successfully exhibited strong enhancement, ranging from 600 to 1200 nm. J_{SC} increased by 31% with further improvement requiring more uniform thickness of the films [235].

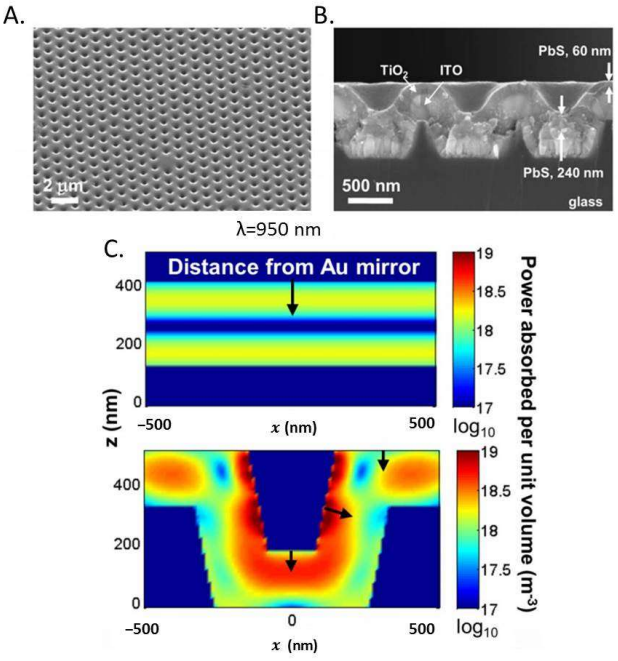

Fig. 6. (A) Forty-five degree tilt angle and (B) cross-sectional scanning electron microscope images of a periodically patterned glass/ITO/TiO_2 solar cell electrode with conformal PbS CQD layer coating. (C) Finite difference time domain simulation of power absorbed per unit volume in a planar PbS CQD solar cell film (top) and a nanostructured PbS CQD solar cell film (bottom) at λ = 950 nm. The two structures have the same total PbS CQD volume. Reprinted with permission from [235]. Copyright 2013 Macmillan Publishers Ltd.

Light trapping techniques that rely on purely geometrical effects instead of device structuring have also been used in CQD solar cells. A metal back mirror was deposited to create a folded light path (FLP) in one CQD solar cell study [236]. Compared with the conventional double-pass absorption scenario at normal incidence, the folded-light-path structure (Figure 7) achieved a total of six light-passes through the active layer, which greatly increased the total path length for photons inside the solar cell. Calculations demonstrated that 50 degrees was an optimal tilt angle, and short-circuit current additions of 3 mA/cm^2 over a planar device were achieved using this design. The overall PCE was increased to 7.8%, despite a slight decrease in open-circuit voltage due to the larger effective device area. The authors of the study predicted that minimizing parasitic absorption in the electrodes by using the best-known TiO_2, ITO and substrate materials could result in short-circuit current densities exceeding 34 mA/cm^2, approaching the theoretical limits for the band gap of the absorber.

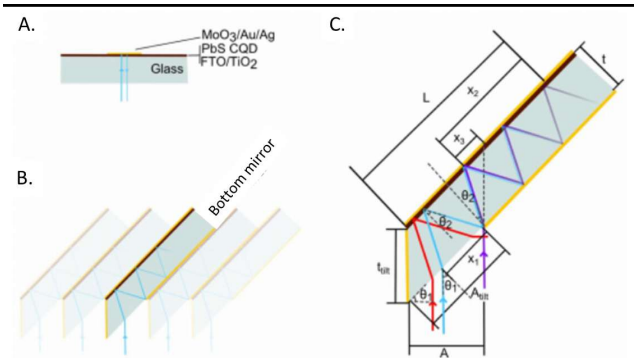

Fig. 7. Configuration and geometric considerations in FLP CQD solar cells. (A) Conventional double-pass CQD solar cell configuration. (B) Periodic arrangement of FLP CQD solar cells. (C) Geometric considerations for multipass absorption in the FLP cell. Reprinted with permission from [236]. Copyright 2013 Macmillan Publishers Ltd.

Another study used an inverted architecture with a ZnO optical spacer to engineer the spatial optical field profile in a CQD solar cell, leading to increased light absorption in the active layer [237]. A low-temperature synthesis process was used for the ZnO so that it could be deposited on top of the CQD layer without degrading the electrical properties of the device. The effect of the spacer layer on the short-circuit current density was dependent on the thicknesses of both the ZnO and PbS CQD layers, which were adjusted to locate the constructive interference within the CQD layer. The inverted architecture and ZnO deposition process introduced some compromises to the electrical performance of the device.

3.1.7 Plasmonically enhanced CQD solar cells

Plasmonics is a rapidly emerging technology of interest for increasing absorption in photovoltaics [238, 239]. Metal nanostructures can be used to confine light to nanoscale dimensions for absorption enhancement via near-field effects or can be used as plasmonic scatterers in far-field light trapping schemes. These properties, along with the ability to seamlessly integrate solution-processed metal nanoparticles into CQD films, make plasmonics a promising method for overcoming the absorption-extraction compromise in CQD solar cells.

In practice, plasmonic materials can act as recombination centers within a semiconducting film, reducing the charge carrier density within a solar cell. Additionally, most plasmonic materials are sources of parasitic absorption. Therefore, materials composition, plasmonic nanoparticle size and shape, and placement within the solar cell of the plasmonic elements need to be carefully designed in order to obtain real improvements in device performance.

One study identified spherical SiO_2-Au core-shell plasmonic structures as being of interest for CQD solar cell integration due to their large scattering-to-absorption ratios [240]. Figure 8 shows a transmission electron microscopy (TEM) image of the well-defined core-shell structure. In the study, CQD devices with integrated Au nanorods exhibited no increase of the short-circuit current density due to parasitic absorption loss introduced by the nanorods. By introducing Au nanoshells, absorption was enhanced by 100% near the plasmon resonance wavelength over nonplasmonic CQD devices. As a result, the overall PCE was increased to 6.9%, an 11% improvement over the reference cell.

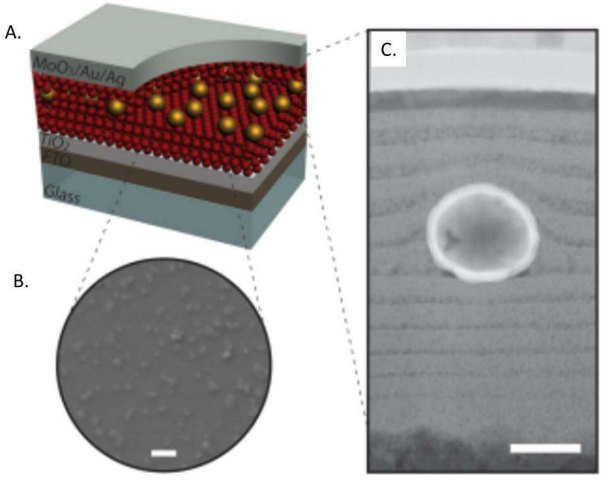

Fig. 8. Plasmonic–excitonic solar cell device design. (A) Schematic of the PbS CQD DH device with embedded nanoshells. (B) Top view scanning electron microscope image showing representative density of nanoshells after CQD deposition. Scale bar, 1 μm. (c) Cross-sectional TEM image showing a single gold nanoshell embedded in a PbS CQD film. Scale bar, 100 nm. Reprinted with permission from [240] Copyright 2013 American Chemical Society.

Another demonstration deployed Ag nanocubes in a BH ZnO nanowire-PbS CQD solar cell to enhance absorption through both near- and far-field scattering [241]. The nanocubes had edge lengths of 80 nm and a radius of curvature of 10 nm and were designed to exhibit a localized surface plasmon resonance (LSPR) between 700–1200 nm, the spectral range where the PbS CQD film was weakly absorbing. The position of the cubes within the cell was important; they were placed far from the front FTO electrode in order to avoid blocking visible light from entering the cell. In addition to the expected increase in J_{SC}, the device $V_{OC}$and FF were also improved through higher carrier extraction efficiency.

Plasmonic nanoparticles have the ability to drastically enhance electric field intensities within their near fields and can therefore in theory be used in light-trapping schemes that exceed the maximum classical thin-film absorption enhancement factor of $4n^2$, where n is the refractive index of the absorbing medium [239, 242]. One study developed plasmonic solar cells which took advantage of the near-field effect in 5 nm Au nanoparticles [243]. Hot electron transfer directly from the excited plasmonic Au nanoparticles to the PbS CQD medium was optimized by the integration of a wide band gap semiconductor (CdS) to passivate the plasmonic nanoparticles. This design reduced carrier scattering while improving the stability of the heat-sensitive films.

Plasmonic grating couplers have also been effective in trapping light in CQD solar cells through the use of surface plasmon polaritons [244]. Plasmonic gratings can be easily integrated into devices through nanostructuring of the metal electrodes. Gratings can be designed to have a large overlap between the diffraction order and metal nanoparticle resonances to efficiently couple light into the active layer of a cell, resulting in increased light absorption and photocurrent. As with integrated plasmonic nanoparticles, however, care must be taken to minimize Ohmic losses associated with parasitic absorption in the metals. A simulation study found that Au nanoparticles with diameters of 140 nm could exhibit strong coupling and lead to an EQE enhancement at the excitonic peak of a CQD solar cell [244].

In addition to providing optical enhancements, plasmonic elements can be used as electrodes in CQD cells. Plasmonic Ag nanoparticles have been used to form a Schottky nanojunction with a PbS CQD film in a photovoltaic device [245]. Both small (40 nm diameter) and large (120 nm diameter) Ag nanoparticles were produced by an evaporative self-assembly technique. The smaller particles had an LSPR at 850 nm, and the larger particles exhibited an EQE enhancement at shorter wavelengths due to a Fabry–Pérot resonance at 580 nm that their inclusion induced in the solar cell.

3.1.8 Multijunction solar cells incorporating CQDs

Multijunction or tandem solar cells are a successful strategy for overcoming the single-junction Shockley–Queisser efficiency limit [246, 247]. Typically, they are composed of stacked series-connected single junction solar cells with different band gaps in which each active layer harvests part of the solar spectrum. CQDs are considered particularly promising materials for multijunction solar cells since their band gaps can be tuned via the quantum size effect throughout the visible and IR portions of the electromagnetic spectrum.

Two main requirements must be considered in designing an efficient tandem CQD solar cell. First, the individual low and high band gap cells must be current-matched which can be achieved by adjusting the active layer thicknesses. The second criterion is making sure that holes from the front cell can recombine with electrons from the back cell efficiently without severe potential loss. Tunnel junctions or recombination layers have been introduced in tandem cells in other materials systems to achieve this second goal [41, 44].

One of the first all-CQD tandem devices employed series connected PbS CQD-TiO_2 cells with a graded recombination layer (GRL) [41]. Instead of using a deep work function contact between the cells, the GRL consisted of thin layers of sputtered MoO_3, ITO and aluminum-doped zinc oxide (AZO). Stacked in that order, the three metal oxide layers exhibited a gradual decrease of work function with MoO_3 and AZO matching the work function of the PbS CQD and TiO_2 films, respectively. The overall open-circuit voltage of the tandem cell (1.06 V) in this demonstration was approximately equal to the sum of the open-circuit voltages of the two constituent single junction cells. With a J_{SC} of 8.3 mA/cm^2, the tandem cell achieved a PCE of 4.21%.

Transparent n-type oxide layers are good candidate materials for graded doping layers in CQD tandem cells, thanks to their favorable doping levels and work functions [191]. Oxides with high doping levels exhibit tunneling-dominant transport while thermionic transport mechanisms are dominant at low doping levels. For a single-material recombination layer strategy, shallow work function materials are preferred, since deep work function materials would exceed the barrier limit for tunneling transport (0.75 eV).

Another early CQD tandem cell demonstration was based on a solution-processed PbS CQD-ZnO design incorporating a metal-based recombination layer [44]. Taking inspiration from organic tandem solar cells, this design used a Au (1 nm)/pH-neutral poly(3,4-ethylenedioxythiophene) (PEDOT) polystyrene sulfonate interlayer. The Au layer was inserted to compensate for the large band offset between PEDOT and ZnO. The tandem cell exhibited a V_{OC} of 0.91 V, a J_{SC} of 3.7 mA/cm^2 and a PCE of 1.27%. Other metal interlayers such as Ag and Al were also attempted, but instead of forming Ohmic contacts, they induced a large series resistance, which deteriorated the device performance.

The high absorption coefficient in the visible portion of the spectrum seen in CQD films makes current matching in all-CQD multijunction cells difficult. Narrow band gap polymers offer complementary absorption properties that can be used in conjunction with CQD films to form hybrid tandem architectures. A blend of poly(3-hexylthiophene) (P3HT) and PCBM was used as the back subcell in a hybrid tandem device that included an interlayer consisting of WO_3 and Al [249]. The limiting factor in the device J_{SC} was the low current produced in the back subcell. Optimization of the thicknesses of both the PbS CQD and P3HT:PCBM layers resulted in better current matching, relatively high V_{OC}, and 1.8% PCE. Though the efficiency in this device was not competitive with the best CQD-only tandem demonstrations, improvements could be made in the organic active layers used as the front subcells. This includes using smaller band gap organic materials such as poly[2,6-(4,4-*bis*-(2-ethylhexyl)-4H-cyclopenta[2,1-b;3,4-b 0]-dithiophene)-alt-4,7-(2,1,3-benzothiadiazole)].

In the highest performing single junction CQD solar cells, efficient electron injection from the CQDs into the n-type material (usually TiO_2 or ZnO) is determined by the band alignment at the heterojunction interface. Hence, it is difficult to optimize small band gap single junction CQD solar cell performance in a heterojunction architecture, because the lowering of the conduction band edge in small band gap CQD films results in unfavorable conditions for charge injection. The results of studies that have been done on optimizing performance in single junction solar cells employing CQD films with band gaps near 1 eV are summarized in Table 2.

3.1.9 Multiple exciton generation

In addition to tandem architectures, MEG can be used as a mechanism for overcoming the single-junction Shockley–Queisser efficiency limit that is of particular interest in CQD solar cells. In semiconductors, when a photon with energy greater than twice the band gap energy is absorbed, multiple electron-hole pairs can be generated if momentum conservation conditions are satisfied. This process is of interest for solar cells since one photon can potentially produce more than one photocarrier pair, leading to

Table 2. Summary of selected optimized studies in single junction CQD solar cells with band gaps near 1 eV.

Structure	CQD material	Band gap (eV)	V_{OC} (V)	J_{SC} (mA/cm^2)	FF (%)	PCE (%)
Depleted heterojunction [181]	PbS	0.9	0.38	11.3	21	0.93
Depleted heterojunction [250]	PbS	1.0	0.4	17.4	58	4
Schottky [251]	$PbS_{0.7}Se_{0.3}$	1.0	0.45	15	50	3.3
Depleted heterojunction [73]	PbS	1.0	0.44	23.8	61.2	5.35
Depleted heterojunction [252]	PbS	0.95	0.48	31	52	7.3

quantum efficiencies exceeding 100%. This process is predicted to be more efficient in quantum confined nanostructures, such as CQDs, because momentum conservation conditions are relaxed in these structures and competing phonon scattering processes are reduced [60]. Transient absorption spectroscopy has been used to study MEG in CQDs and obtain quantum yields [60, 253, 254]. Various studies on quantum confined materials including PbSe, PbS, CdSe, $CuInSe_2$ and PbS_xSe_{1-x} alloyed CQDs have measured MEG processes with different thresholds and quantum yields [60, 254, 255].

The first CQD solar cell demonstrating MEG was reported in 2011. It showed a peak EQE of greater than 100% at short wavelengths, with a maximum value of 114% [256]. A BH architecture employing MEG was used to enhance carrier extraction. The key to achieving high MEG efficiency was a ligand exchange process employing hydrazine. Devices that used hydrazine-treated PbSe CQDs, as opposed to those using conventional dithiol treatments, showed improvements in all solar cell parameters, including J_{SC}, V_{OC},FF and PCE. The MEG device internal quantum efficiency (IQE) was obtained from the EQE measurements, taking into account absorption and reflectance in the cell. The IQE reached a peak of 130% at short wavelengths in cells using CQDs with a band gap of 0.72 eV. To maximize the performance effects, developing materials engineering strategies that move the MEG threshold closer to twice the band gap energy will be important.

To further understand and increase the MEG efficiency, studies have been done on nanocrystals with various shapes, sizes and surface ligands [253, 257–259]. Related studies on measuring hot electron cooling rates using transient absorption spectroscopy have also been conducted [260]. One study observed slower cooling rates in PbSe/CdSe core-shell nanostructures along with high MEG yields and lower MEG threshold energies [261]. The authors attributed this improvement over core-only structures to the interaction of valence band states between the core and shell.

Singlet exciton fission is an analogous process to MEG that can occur in organic semiconductors, although extracting the low-energy triplet products is a challenge. Several recent experiments have demonstrated the efficient transfer of the triplet products of singlet exciton fission in organic materials to CQD materials in hybrid architectures. One study observed multiple triplet exciton generation in pentacene followed by transport to PbSe CQDs via Dexter transfer [262]. The transfer process was only efficient when the band gap of the PbSe CQD material was in resonance with the energy of the triplet excitons. Another study observed triplet transfer from tetracene to size-tuned PbS CQDs [263]. Shorter ligands were also found to facilitate higher transfer efficiency. By using singlet fission, the PCE in hybrid organic-inorganic architectures can in theory be enhanced through additional photocurrent generation.

3.1.10 Luminescent solar concentrators

Luminescent solar concentrators (LSCs) have been developed in parallel with photovoltaics as an alternative strategy for covering large areas with solar-harvesting materials. The key component of LSCs is a dye or other luminescent material that absorbs and then re-emits light, which is directed through a waveguide to a relatively small solar cell for conversion into electricity. The use of LSCs in theory decouples light collection and charge transport, and allows for the collection of both direct and diffuse light without the need for tracking or scaling of expensive solar cells over large areas. CQDs have been proposed as a promising candidate material for LSCs.

There are several optical design challenges associated with building efficient LSCs. These include minimization of reflection and transmission losses in the system, as well as high luminescence quantum efficiency. Importantly, the luminescent materials need to exhibit broadband absorption and minimal spectral overlap between their absorption and emission in order to minimize reabsorption. Recently, CQDs with both broadband absorption and high photoluminescence quantum efficiency have been investigated as a promising candidates for use in LCS. The main obstacle for developing CQDs as LSC materials is their relatively small Stokes shifts (spectral separation between ab-

sorption and emission bandwidths), which are associated with large reabsorption probability [264].

One of the strategies to reduce reabsorption in CQDs is by doping them with metal ions and using the resulting lower energy intraband gap states for emission. Doping effectively alleviates reabsorption by increasing the Stokes shift in the CQDs. However, doping can also lower the quantum yields (to less than 30%), which negatively impacts the overall conversion efficiency [265].

Another promising approach is to employ core-shell quantum dots with type II heterostructures to tune the Stokes shift. A CdSe/CdS core-shell CQD was proposed to spectrally separate absorption and emission processes [266]. The thickness of the CdS shell was designed to isolate the inner CdSe core and effectively reduce nonradiative recombination. A Stokes shift of larger than 400 MeV was observed in the core-shell photoluminescence spectra, compared with a Stokes shift of about 70 MeV for CdSe core-only quantum dots. As a result, a 100-fold increase in the number of photons reaching the solar cell in a LSC setup was achieved. Another study on the CdSe/CdS core-shell CQD system used a modified synthesis procedure to achieve a doubled 82% quantum yield compared with the thick shell CQDs [267]. The absorption efficiency was 48% in that system, with optical losses attributed to other effects such as reflection, transmittance and nonuniform quantum yield.

Another demonstration used Mn^{2+}-doped ZnSe/ZnS core-shell CQD structures in a LSC system [268]. Due to a large difference in the absorptivity between the Mn^{2+} ion inclusions and the ZnSe, a Stokes shift of 1 eV was obtained. The photoluminescence quantum efficiency of the CQDs was nearly 53% and further improvements were predicted to be possible by optimizing the CQD passivation. A $Cd_{1-x}Cu_xSe$ CQD materials system with an even narrower band gap was employed to fully utilize the solar spectrum [269]. Thanks to both high absorption and little overlap between the absorption and emission spectra, it compared favorably with CdSe/CdS core-shell, CdSe/CdS dot-in-rod and $Zn_{0.87}Cd_{0.11}Mn_{0.02}Se$/ZnS demonstrations [269]. Other CQD LSC demonstrations include ternary I–III–VI_2 CISeS materials [270], which exhibited high absorption and a large Stokes shift of 530 MeV.

Apart from the radiative quantum efficiency of the luminescent materials, the waveguide used in LSC systems is another potential source of light loss. CdSe/CdS CQDs were used in combination with a photonic mirror which assisted in trapping the emitted light inside the waveguide [271]. The photonic mirror allowed the portion of the light that was not trapped by total internal reflection or scattered to be efficiently harnessed. A 60% photoluminescence efficiency was demonstrated, and a high concentration factor of 30 was achieved in that system.

4 Conclusions and perspectives

CQD solar cell efficiencies have improved dramatically in a single decade, from their inception in 2005 to the highest certified PCEs today of 9.9%. The field still holds great potential for further improvements, which will require a systematic understanding of intrinsic transport mechanisms, wise architecture design and the incorporation of advanced nanotechnology concepts. Improving transport in CQD thin films remains the greatest challenge in realizing single junction efficiencies of 15–20% that are comparable to crystalline thin film technologies.

In the materials engineering sphere, the large electronic trap state densities in CQD films impede efficient transport and limit solar cell V_{OC}. Novel materials with better surface passivation must be engineered, given that most of the trap states are attributed to imperfectly passivated nanocrystal surface sites. Carrier mobilities are still limited to the 10^{-3} to 10^{-2} $cm^2/V/s$ range, which is well below those found in the best-performing traditional semiconductor solar cells materials. Diffusion lengths must also be improved. There is evidence that transport in CQD films is largely trap-limited and that improving this aspect of the materials will simultaneously lead to higher mobilities and diffusion lengths [272].

Developing solar cell architectures that deploy the unique properties of CQDs, in combination with band engineering, is a promising way to enhance carrier extraction and achieve large photocurrents. However, methods to improve carrier extraction can introduce detrimental side effects, including additional series resistance or interface recombination. Other strategies that rely on complicated fabrication procedures detract from the scalability of solution-based processing methods as a selling point of CQD materials. Therefore, it is important to take a comprehensive view of device design when developing new solar cell architectures.

Photon management, including integrating plasmonic elements, continues to be a promising avenue to increasing performance in CQD solar cells. New plasmonic enhancement strategies will require the design of the materials and structures that maximize field enhancement in the active material while minimizing parasitic absorption in the plasmonic elements themselves to achieve a net increase in J_{SC}. Developing other hybrid materials and photonic strategies that allow absorption in CQD films

to be better matched to the solar spectrum through complementary functionality is another promising research avenue.

Although CQD solar cell efficiencies are reaching parity with other solution-processed photovoltaic materials, much of the promise of this materials system lies in its potential to be used in hybrid strategies for overcoming the traditional single-junction efficiency limits. Recent demonstrations combining CQDs with other materials, including transfer of spin triplets generated through singlet fusion in pentacene [262] and tetracene [263] to PbSe and PbS CQDs, as well as heteroepitaxially grown CQD hybrids [273], should lead to next-generation device applications. The band gap tunability and solution-processed deposition of CQDs make them of particular interest for use as IR layers in multijunction strategies with other materials acting as the visible cells. Additionally, exploitation of MEG in CQD films has received much interest due to recent demonstrations of greater-than-unity IQE in CQD solar cells [256]. In order to achieve real PCE gains, understanding the fundamental processes affecting MEG yields will be critical, as will developing schemes to suppress fast relaxation processes and improve carrier extraction.

In conclusion, CQDs remain a promising material set for scalable photovoltaic technologies, as well as an intriguing test-bed for studying fundamental processes involved in nanoscale energy generation and transport.

References

[1] Colvin VL, Schlamp MC, Alivisatos AP. Light-emitting diodes made from cadmium selenide nanocrystals and a semiconducting polymer. Nature 1994, 370, 354–7.

[2] Tessler N, Medvedev V, Kazes M, Kan S, Banin U. Efficient Near-Infrared Polymer Nanocrystal Light-Emitting Diodes. Science 2002, 295, 1506–8.

[3] Caruge JM, Halpert JE, Wood V, Bulović V, Bawendi MG. Colloidal quantum-dot light-emitting diodes with metal-oxide charge transport layers. Nat Photonics 2008, 2, 247–50.

[4] Shirasaki Y, Supran GJ, Bawendi MG, Bulović V. Emergence of colloidal quantum-dot light-emitting technologies. Nat Photonics 2013, 7, 13–23.

[5] Sun Q, Wang YA, Li LS, et al. Bright, multicoloured light-emitting diodes based on quantum dots. Nat Photonics 2007, 1, 717–22.

[6] Konstantatos G, Howard I, Fischer A, et al. Ultrasensitive solution-cast quantum dot photodetectors. Nature 2006, 442, 180–3.

[7] Konstantatos G, Sargent EH. Colloidal quantum dot photodetectors. Infrared Phys Technol 2011, 54, 278–82.

[8] Sukhovatkin V, Hinds S, Brzozowski L, Sargent EH. Colloidal Quantum-Dot Photodetectors Exploiting Multiexciton Generation. Science 2009, 324, 1542–4.

[9] Clifford JP, Konstantatos G, Johnston KW, Hoogland S, Levina L, Sargent EH. Fast, sensitive and spectrally tuneable colloidal-quantum-dot photodetectors. Nat Nanotechnol 2009, 4, 40–4.

[10] Alivisatos AP, Gu W, Larabell C. Quantum Dots as Cellular Probes. Annu Rev Biomed Eng 2005, 7, 55–76.

[11] Han M, Gao X, Su JZ, Nie S. Quantum-dot-tagged microbeads for multiplexed optical coding of biomolecules. Nat Biotechnol 2001, 19, 631–5.

[12] Chan WCW, Maxwell DJ, Gao X, Bailey RE, Han M, Nie S. Luminescent quantum dots for multiplexed biological detection and imaging. Curr Opin Biotechnol 2002, 13, 40–6.

[13] Medintz IL, Clapp AR, Mattoussi H, Goldman ER, Fisher B, Mauro JM. Self-assembled nanoscale biosensors based on quantum dot FRET donors. Nat Mater 2003, 2, 630–8.

[14] Sapsford KE, Pons T, Medintz IL, Mattoussi H. Biosensing with Luminescent Semiconductor Quantum Dots. Sensors 2006, 6, 925–53.

[15] Barkhouse DAR, Debnath R, Kramer IJ, et al. Depleted Bulk Heterojunction Colloidal Quantum Dot Photovoltaics. Adv Mater 2011, 23, 3134–8.

[16] Tang J, Kemp KW, Hoogland S, et al. Colloidal-quantum-dot photovoltaics using atomic-ligand passivation. Nat Mater 2011, 10, 765–71.

[17] Ip AH, Thon SM, Hoogland S, et al. Hybrid passivated colloidal quantum dot solids. Nat Nanotechnol 2012, 7, 577–82.

[18] Koleilat GI, Levina L, Shukla H, et al. Efficient, Stable Infrared Photovoltaics Based on Solution-Cast Colloidal Quantum Dots. ACS Nano 2008, 2, 833–40.

[19] Jean J, Brown PR, Jaffe RL, Buonassisi T, Bulović V. Pathways for solar photovoltaics. Energy Environ Sci 2015, 8, 1200–19.

[20] Wadia C, Alivisatos AP, Kammen DM. Materials Availability Expands the Opportunity for Large-Scale Photovoltaics Deployment. Environ Sci Technol 2009, 43, 2072–7.

[21] Kramer IJ, Minor JC, Moreno-Bautista G, et al. Efficient Spray-Coated Colloidal Quantum Dot Solar Cells. Adv Mater 2015, 27, 116–21.

[22] Sargent EH. Colloidal quantum dot solar cells. Nat Photonics 2012, 6, 133–5.

[23] Chuang C-HM, Brown PR, Bulović V, Bawendi MG. Improved performance and stability in quantum dot solar cells through band alignment engineering. Nat Mater 2014, 13, 796–801.

[24] Loiudice A, Rizzo A, Corricelli M, et al. Room-temperature treatments for all-inorganic nanocrystal solar cell devices. Thin Solid Films 2014, 560, 44–8.

[25] Ning Z, Voznyy O, Pan J, et al. Air-stable n-type colloidal quantum dot solids. Nat Mater 2014, 13, 822–8.

[26] Zhang J, Gao J, Church CP, et al. PbSe Quantum Dot Solar Cells with More than 6% Efficiency Fabricated in Ambient Atmosphere. Nano Lett 2014, 14, 6010–5.

[27] Tang J, Brzozowski L, Barkhouse DAR, et al. Quantum Dot Photovoltaics in the Extreme Quantum Confinement Regime: The Surface-Chemical Origins of Exceptional Air- and Light-Stability. ACS Nano 2010, 4, 869–78.

[28] Liu H, Li M, Voznyy O, et al. Physically Flexible, Rapid-Response Gas Sensor Based on Colloidal Quantum Dot Solids. Adv Mater 2014, 26, 2718–24.

[29] He J, Luo M, Hu L, et al. Flexible lead sulfide colloidal quantum dot photodetector using pencil graphite electrodes on paper substrates. J Alloys Compd 2014, 596, 73–8.

[30] Jang J, Shim HC, Ju Y, et al. All-solution-processed PbS quantum dot solar modules. Nanoscale 2015, 7, 8829–34.
[31] Chalao Wongsaeng, Singjai P. Mobilities in ambipolar field effect transistors based on single-walled carbon nanotube network and formed on a gold nanoparticle template. Appl Phys Lett 2014, 104, 1–5.
[32] Kramer IJ, Moreno-Bautista G, Minor JC, Kopilovic D, Sargent EH. Colloidal quantum dot solar cells on curved and flexible substrates. Appl Phys Lett 2014, 105, 163902.
[33] Jiang Z, You G, Wang L, et al. Solution-processed high-performance colloidal quantum dot tandem photodetectors on flexible substrates. J Appl Phys 2014, 116, 084303.
[34] Loiudice A, Rizzo A, Grancini G, et al. Fabrication of flexible all-inorganic nanocrystal solar cells by room-temperature processing. Energy Environ Sci 2013, 6, 1565–72.
[35] Tan Z, Xu J, Zhang C, et al. Colloidal nanocrystal-based light-emitting diodes fabricated on plastic toward flexible quantum dot optoelectronics. J Appl Phys 2009, 105, N.PAG.
[36] Kalowekamo J, Baker E. Estimating the manufacturing cost of purely organic solar cells. Sol Energy 2009, 83, 1224–31.
[37] Aroutiounian VM, Petrosyan S, Khachatryan A, Touryan KJ. Quantum dot solar cells. vol. 4458, 2001, p. 38–45.
[38] Klimov VI. Detailed-balance power conversion limits of nanocrystal-quantum-dot solar cells in the presence of carrier multiplication. Appl Phys Lett 2006, 89, 123118.
[39] Baskoutas S, Terzis AF. Size-dependent band gap of colloidal quantum dots. J Appl Phys 2006, 99, 013708.
[40] Shockley W, Queisser HJ. Detailed Balance Limit of Efficiency of p-n Junction Solar Cells. J Appl Phys 1961, 32, 510–9.
[41] Wang X, Koleilat GI, Tang J, et al. Tandem colloidal quantum dot solar cells employing a graded recombination layer. Nat Photonics 2011, 5, 480–4.
[42] Brown AS, Green MA. Detailed balance limit for the series constrained two terminal tandem solar cell. Phys E Low-Dimens Syst Nanostructures 2002, 14, 96–100.
[43] Santra PK, Kamat PV. Tandem-Layered Quantum Dot Solar Cells: Tuning the Photovoltaic Response with Luminescent Ternary Cadmium Chalcogenides. J Am Chem Soc 2013, 135, 877–85.
[44] Choi JJ, Wenger WN, Hoffman RS, et al. Solution-Processed Nanocrystal Quantum Dot Tandem Solar Cells. Adv Mater 2011, 23, 3144–8.
[45] Kramer IJ, Levina L, Debnath R, Zhitomirsky D, Sargent EH. Solar Cells Using Quantum Funnels. Nano Lett 2011, 11, 3701–6.
[46] Tang J, Liu H, Zhitomirsky D, et al. Quantum Junction Solar Cells. Nano Lett 2012, 12, 4889–94.
[47] Freundlich A, Alemu A. Multi quantum well multijunction solar cell for space applications. Phys Status Solidi C 2005, 2, 2978–81.
[48] H. Sargent E. Infrared Quantum Dots. Adv Mater 2005, 17, 515–22.
[49] Azizi SN, Chaichi MJ, Shakeri P, Bekhradnia A. Determination of atropine using Mn-doped ZnS quantum dots as novel luminescent sensitizers. J Lumin 2013, 144, 34–40.
[50] Trevisan R, Rodenas P, Gonzalez-Pedro V, et al. Harnessing Infrared Photons for Photoelectrochemical Hydrogen Generation. A PbS Quantum Dot Based "Quasi-Artificial Leaf." J Phys Chem Lett 2013, 4, 141–6.
[51] Choudhury KR, Sahoo Y, Ohulchanskyy TY, Prasad PN. Efficient photoconductive devices at infrared wavelengths using quantum dot-polymer nanocomposites. Appl Phys Lett 2005, 87, 073110.
[52] McDonald SA, Konstantatos G, Shiguo Zhang, et al. Solution-processed PbS quantum dot infrared photodetectors and photovoltaics. Nat Mater 2005, 4, 138–42.
[53] Wang H, Li Z, Fu C, et al. Solution-Processed PbSe Colloidal Quantum Dot-Based Near-Infrared Photodetector. IEEE Photonics Technol Lett 2015, 27, 612–5.
[54] Lin K-F, Cheng H-M, Hsu H-C, Lin L-J, Hsieh W-F. Band gap variation of size-controlled ZnO quantum dots synthesized by sol–gel method. Chem Phys Lett 2005, 409, 208–11.
[55] Fonoberov VA, Pokatilov EP, Balandin AA. Exciton states and optical transitions in colloidal CdS quantum dots: Shape and dielectric mismatch effects. Phys Rev B 2002, 66, 085310.
[56] Kongkanand A, Tvrdy K, Takechi K, Kuno M, Kamat PV. Quantum Dot Solar Cells. Tuning Photoresponse through Size and Shape Control of CdSe–TiO_2 Architecture. J Am Chem Soc 2008, 130, 4007–15.
[57] Choi H, Ko J-H, Kim Y-H, Jeong S. Steric-Hindrance-Driven Shape Transition in PbS Quantum Dots: Understanding Size-Dependent Stability. J Am Chem Soc 2013, 135, 5278–81.
[58] Hines MA, Scholes GD. Colloidal PbS Nanocrystals with Size-Tunable Near-Infrared Emission: Observation of Post-Synthesis Self-Narrowing of the Particle Size Distribution. Adv Mater 2003, 15, 1844–9.
[59] Owen JS, Chan EM, Liu H, Alivisatos AP. Precursor Conversion Kinetics and the Nucleation of Cadmium Selenide Nanocrystals. J Am Chem Soc 2010, 132, 18206–13.
[60] Ellingson RJ, Beard MC, Johnson JC, et al. Highly Efficient Multiple Exciton Generation in Colloidal PbSe and PbS Quantum Dots. Nano Lett 2005, 5, 865–71.
[61] Nozik AJ. Multiple exciton generation in semiconductor quantum dots. Chem Phys Lett 2008, 457, 3–11.
[62] Ekuma CE, Singh DJ, Moreno J, Jarrell M. Optical properties of PbTe and PbSe. Phys Rev B 2012, 85, 085205.
[63] Yeh M-H, Lin L-Y, Lee C-P, et al. High performance CdS quantum-dot-sensitized solar cells with Ti-based ceramic materials as catalysts on the counter electrode. J Power Sources 2013, 237, 141–8.
[64] Robel I, Subramanian V, Kuno M, Kamat PV. Quantum Dot Solar Cells. Harvesting Light Energy with CdSe Nanocrystals Molecularly Linked to Mesoscopic TiO_2 Films. J Am Chem Soc 2006, 128, 2385–93.
[65] Park J, Joo J, Kwon SG, Jang Y, Hyeon T. Synthesis of Monodisperse Spherical Nanocrystals. Angew Chem Int Ed 2007, 46, 4630–60.
[66] Murray CB, Norris DJ, Bawendi MG. Synthesis and characterization of nearly monodisperse CdE (E = sulfur, selenium, tellurium) semiconductor nanocrystallites. J Am Chem Soc 1993, 115, 8706–15.
[67] Burda C, Chen X, Narayanan R, El-Sayed MA. Chemistry and Properties of Nanocrystals of Different Shapes. Chem Rev 2005, 105, 1025–102.
[68] Moreels I, Justo Y, De Geyter B, Haustraete K, Martins JC, Hens Z. Size-Tunable, Bright, and Stable PbS Quantum Dots: A Surface Chemistry Study. ACS Nano 2011, 5, 2004–12.

[69] Kwon SG, Piao Y, Park J, et al. Kinetics of Monodisperse Iron Oxide Nanocrystal Formation by "Heating-Up" Process. J Am Chem Soc 2007, 129, 12571–84.
[70] Park J, An K, Hwang Y, et al. Ultra-large-scale syntheses of monodisperse nanocrystals. Nat Mater 2004, 3, 891–5.
[71] Ma W, Swisher SL, Ewers T, et al. Photovoltaic Performance of Ultrasmall PbSe Quantum Dots. ACS Nano 2011, 5, 8140–7.
[72] Zhang J, Gao J, Miller EM, Luther JM, Beard MC. Diffusion-Controlled Synthesis of PbS and PbSe Quantum Dots with in Situ Halide Passivation for Quantum Dot Solar Cells. ACS Nano 2014, 8, 614–22.
[73] Yuan M, Kemp KW, Thon SM, et al. High-Performance Quantum-Dot Solids via Elemental Sulfur Synthesis. Adv Mater 2014, 26, 3513–9.
[74] McPhail MR, Weiss EA. Role of Organosulfur Compounds in the Growth and Final Surface Chemistry of PbS Quantum Dots. Chem Mater 2014, 26, 3377–84.
[75] Lipovskii A, Kolobkova E, Petrikov V, et al. Synthesis and characterization of PbSe quantum dots in phosphate glass. Appl Phys Lett 1997, 71, 3406–8.
[76] Borrelli NF, Smith DW. Quantum confinement of PbS microcrystals in glass. J Non-Cryst Solids 1994, 180, 25–31.
[77] Yan X, Cui X, Li L. Synthesis of Large, Stable Colloidal Graphene Quantum Dots with Tunable Size. J Am Chem Soc 2010, 132, 5944–5.
[78] Micic OI, Curtis CJ, Jones KM, Sprague JR, Nozik AJ. Synthesis and Characterization of InP Quantum Dots. J Phys Chem 1994, 98, 4966–9.
[79] Nordell KJ, Boatman EM, Lisensky GC. A Safer, Easier, Faster Synthesis for CdSe Quantum Dot Nanocrystals. J Chem Educ 2005, 82, 1697.
[80] Guzelian AA, Banin U, Kadavanich AV, Peng X, Alivisatos AP. Colloidal chemical synthesis and characterization of InAs nanocrystal quantum dots. Appl Phys Lett 1996, 69, 1432–4.
[81] Nose K, Omata T, Otsuka-Yao-Matsuo S. Colloidal Synthesis of Ternary Copper Indium Diselenide Quantum Dots and Their Optical Properties. J Phys Chem C 2009, 113, 3455–60.
[82] Smith DK, Luther JM, Semonin OE, Nozik AJ, Beard MC. Tuning the Synthesis of Ternary Lead Chalcogenide Quantum Dots by Balancing Precursor Reactivity. ACS Nano 2011, 5, 183–90.
[83] Deng Z, Yan H, Liu Y. Band Gap Engineering of Quaternary-Alloyed ZnCdSSe Quantum Dots via a Facile Phosphine-Free Colloidal Method. J Am Chem Soc 2009, 131, 17744–5.
[84] Wu B-L, Chao H-J, Chen C-P, Yang C-H, Chang J-Y. One-pot synthesis of colloidal Cdx:$CuInS_2$ quaternary quantum dots used as sensitizers in photovoltaic cells. RSC Adv 2015, 5, 36605–13.
[85] Green M. The nature of quantum dot capping ligands. J Mater Chem 2010, 20, 5797–809.
[86] Taylor J, Kippeny T, Rosenthal SJ. Surface Stoichiometry of CdSe Nanocrystals Determined by Rutherford Backscattering Spectroscopy. J Clust Sci 2001, 12, 571–82.
[87] Jasieniak J, Mulvaney P. From Cd-Rich to Se-Rich – the Manipulation of CdSe Nanocrystal Surface Stoichiometry. J Am Chem Soc 2007, 129, 2841–8.
[88] Moreels I, Fritzinger B, Martins JC, Hens Z. Surface Chemistry of Colloidal PbSe Nanocrystals. J Am Chem Soc 2008, 130, 15081–6.
[89] Talapin DV, Lee J-S, Kovalenko MV, Shevchenko EV. Prospects of Colloidal Nanocrystals for Electronic and Optoelectronic Applications. Chem Rev 2010, 110, 389–458.
[90] Kovalenko MV, Scheele M, Talapin DV. Colloidal Nanocrystals with Molecular Metal Chalcogenide Surface Ligands. Science 2009, 324, 1417–20.
[91] Guyot-Sionnest P. Electrical Transport in Colloidal Quantum Dot Films. J Phys Chem Lett 2012, 3, 1169–75.
[92] Zabet-Khosousi A, Dhirani A-A. Charge Transport in Nanoparticle Assemblies. Chem Rev 2008, 108, 4072–124.
[93] Uyeda HT, Medintz IL, Jaiswal JK, Simon SM, Mattoussi H. Synthesis of Compact Multidentate Ligands to Prepare Stable Hydrophilic Quantum Dot Fluorophores. J Am Chem Soc 2005, 127, 3870–8.
[94] Klem EJD, Shukla H, Hinds S, MacNeil DD, Levina L, Sargent EH. Impact of dithiol treatment and air annealing on the conductivity, mobility, and hole density in PbS colloidal quantum dot solids. Appl Phys Lett 2008, 92, 212105.
[95] Giansante C, Carbone L, Giannini C, et al. Colloidal Arenethiolate-Capped PbS Quantum Dots: Optoelectronic Properties, Self-Assembly, and Application in Solution-Cast Photovoltaics. J Phys Chem C 2013, 117, 13305–17.
[96] Barkhouse DAR, Pattantyus-Abraham AG, Levina L, Sargent EH. Thiols Passivate Recombination Centers in Colloidal Quantum Dots Leading to Enhanced Photovoltaic Device Efficiency. ACS Nano 2008, 2, 2356–62.
[97] Greaney MJ, Couderc E, Zhao J, et al. Controlling the Trap State Landscape of Colloidal CdSe Nanocrystals with Cadmium Halide Ligands. Chem Mater 2015, 27, 744–56.
[98] Jiang C, Lee J-S, Talapin DV. Soluble Precursors for CuInSe2, $CuIn_{1-x}Ga_xSe_2$, and $Cu_2ZnSn(S,Se)_4$ Based on Colloidal Nanocrystals and Molecular Metal Chalcogenide Surface Ligands. J Am Chem Soc 2012, 134, 5010–3.
[99] Lee J-S, Kovalenko MV, Huang J, Chung DS, Talapin DV. Band-like transport, high electron mobility and high photoconductivity in all-inorganic nanocrystal arrays. Nat Nanotechnol 2011, 6, 348–52.
[100] Ning Z, Dong H, Zhang Q, Voznyy O, Sargent EH. Solar Cells Based on Inks of n-Type Colloidal Quantum Dots. ACS Nano 2014, 8, 10321–7.
[101] Neo DCJ, Cheng C, Stranks SD, et al. Influence of Shell Thickness and Surface Passivation on PbS/CdS Core/Shell Colloidal Quantum Dot Solar Cells. Chem Mater 2014, 26, 4004–13.
[102] efficiency_chart.jpg (4190×2456) n.d. http://www.nrel.gov/ncpv/images/efficiency_chart.jpg (accessed September 7, 2015).
[103] Kirmani AR, Carey GH, Abdelsamie M, et al. Effect of Solvent Environment on Colloidal-Quantum-Dot Solar-Cell Manufacturability and Performance. Adv Mater 2014, 26, 4717–23.
[104] Cassagneau T, Mallouk TE, Fendler JH. Layer-by-Layer Assembly of Thin Film Zener Diodes from Conducting Polymers and CdSe Nanoparticles. J Am Chem Soc 1998, 120, 7848–59.
[105] Liu Y, Gibbs M, Puthussery J, et al. Dependence of Carrier Mobility on Nanocrystal Size and Ligand Length in PbSe Nanocrystal Solids. Nano Lett 2010, 10, 1960–9.
[106] Lee J-W, Son D-Y, Ahn TK, et al. Quantum-Dot-Sensitized Solar Cell with Unprecedentedly High Photocurrent. Sci Rep 2013, 3.

[107] Luther JM, Law M, Beard MC, et al. Schottky Solar Cells Based on Colloidal Nanocrystal Films. Nano Lett 2008, 8, 3488–92.
[108] Dilena E, Xie Y, Brescia R, et al. $CuIn_xGa_{1-x}S_2$ Nanocrystals with Tunable Composition and Band Gap Synthesized via a Phosphine-Free and Scalable Procedure. Chem Mater 2013, 25, 3180–7.
[109] Keuleyan S, Lhuillier E, Guyot-Sionnest P. Synthesis of Colloidal HgTe Quantum Dots for Narrow Mid-IR Emission and Detection. J Am Chem Soc 2011, 133, 16422–4.
[110] Steinhagen C, Panthani MG, Akhavan V, Goodfellow B, Koo B, Korgel BA. Synthesis of Cu_2ZnSnS_4 Nanocrystals for Use in Low-Cost Photovoltaics. J Am Chem Soc 2009, 131, 12554–5.
[111] Im SH, Lee YH, Seok SI, Kim SW, Kim S-W. Quantum-Dot-Sensitized Solar Cells Fabricated by the Combined Process of the Direct Attachment of Colloidal CdSe Quantum Dots Having a ZnS Glue Layer and Spray Pyrolysis Deposition. Langmuir 2010, 26, 18576–80.
[112] Carey GH, Kramer IJ, Kanjanaboos P, et al. Electronically Active Impurities in Colloidal Quantum Dot Solids. ACS Nano 2014, 8, 11763–9.
[113] Chen M, Yu H, Kershaw SV, et al. Fast, Air-Stable Infrared Photodetectors based on Spray-Deposited Aqueous HgTe Quantum Dots. Adv Funct Mater 2014, 24, 53–9.
[114] Bodnarchuk MI, Kovalenko MV, Pichler S, Fritz-Popovski G, Hesser G, Heiss W. Large-Area Ordered Superlattices from Magnetic Wüstite/Cobalt Ferrite Core/Shell Nanocrystals by Doctor Blade Casting. ACS Nano 2010, 4, 423–31.
[115] Rauch T, Böberl M, Tedde SF, et al. Near-infrared imaging with quantum-dot-sensitized organic photodiodes. Nat Photonics 2009, 3, 332–6.
[116] Fischer A, Rollny L, Pan J, et al. Directly Deposited Quantum Dot Solids Using a Colloidally Stable Nanoparticle Ink. Adv Mater 2013, 25, 5742–9.
[117] Norris DJ, Bawendi MG. Measurement and assignment of the size-dependent optical spectrum in CdSe quantum dots. Phys Rev B 1996, 53, 16338–46.
[118] Bailey RE, Nie S. Alloyed Semiconductor Quantum Dots: Tuning the Optical Properties without Changing the Particle Size. J Am Chem Soc 2003, 125, 7100–6.
[119] Zheng J, Zhang C, Dickson RM. Highly Fluorescent, Water-Soluble, Size-Tunable Gold Quantum Dots. Phys Rev Lett 2004, 93, 077402.
[120] Brus L. Electronic wave functions in semiconductor clusters: experiment and theory. J Phys Chem 1986, 90, 2555–60.
[121] Moreels I, Lambert K, Smeets D, et al. Size-Dependent Optical Properties of Colloidal PbS Quantum Dots. ACS Nano 2009, 3, 3023–30.
[122] Miller OD, Yablonovitch E, Kurtz SR. Strong Internal and External Luminescence as Solar Cells Approach the Shockley #x2013;Queisser Limit. IEEE J Photovolt 2012, 2, 303–11.
[123] Klimov VI, Mikhailovsky AA, Xu S, et al. Optical Gain and Stimulated Emission in Nanocrystal Quantum Dots. Science 2000, 290, 314–7.
[124] Voznyy O. Mobile Surface Traps in CdSe Nanocrystals with Carboxylic Acid Ligands. J Phys Chem C 2011, 115, 15927–32.
[125] Liu Y-F, Yu J-S. Selective synthesis of CdTe and high luminescence CdTe/CdS quantum dots: The effect of ligands. J Colloid Interface Sci 2009, 333, 690–8.
[126] Silva FO, Carvalho MS, Mendonça R, et al. Effect of surface ligands on the optical properties of aqueous soluble CdTe quantum dots. Nanoscale Res Lett 2012, 7, 1–10.
[127] Smith AR, Yoon W, Heuer WB, et al. Effect of Ligand Structure on the Optical and Electronic Properties of Nanocrystalline PbSe Films. J Phys Chem C 2012, 116, 6031–7.
[128] Xu F, Gerlein LF, Ma X, Haughn CR, Doty MF, Cloutier SG. Impact of Different Surface Ligands on the Optical Properties of PbS Quantum Dot Solids. Materials 2015, 8, 1858–70.
[129] Luque A, Martí A, Nozik AJ. Solar Cells Based on Quantum Dots: Multiple Exciton Generation and Intermediate Bands. MRS Bull 2007, 32, 236–41.
[130] Beard MC. Multiple Exciton Generation in Semiconductor Quantum Dots. J Phys Chem Lett 2011, 2, 1282–8.
[131] Jung HK, Taniguchi K, Hamaguchi C. Impact ionization model for full band Monte Carlo simulation in GaAs. J Appl Phys 1996, 79, 2473.
[132] Luther JM, Beard MC, Song Q, Law M, Ellingson RJ, Nozik AJ. Multiple Exciton Generation in Films of Electronically Coupled PbSe Quantum Dots. Nano Lett 2007, 7, 1779–84.
[133] Jeong KS, Tang J, Liu H, et al. Enhanced Mobility-Lifetime Products in PbS Colloidal Quantum Dot Photovoltaics. ACS Nano 2012, 6, 89–99.
[134] Carey GH, Levina L, Comin R, Voznyy O, Sargent EH. Record Charge Carrier Diffusion Length in Colloidal Quantum Dot Solids via Mutual Dot-To-Dot Surface Passivation. Adv Mater 2015, 27, 3325–30.
[135] Zhitomirsky D, Voznyy O, Hoogland S, Sargent EH. Measuring Charge Carrier Diffusion in Coupled Colloidal Quantum Dot Solids. ACS Nano 2013, 7, 5282–90.
[136] Bozyigit D, Volk S, Yarema O, Wood V. Quantification of Deep Traps in Nanocrystal Solids, Their Electronic Properties, and Their Influence on Device Behavior. Nano Lett 2013, 13, 5284–8.
[137] Zhang Y, Zherebetskyy D, Bronstein ND, et al. Molecular Oxygen Induced in-Gap States in PbS Quantum Dots. ACS Nano 2015, 9, 10445–52.
[138] Fiore A, Rossetti M, Alloing B, et al. Carrier diffusion in low-dimensional semiconductors: A comparison of quantum wells, disordered quantum wells, and quantum dots. Phys Rev B 2004, 70, 205311.
[139] Maria A, Cyr PW, Klem EJD, Levina L, Sargent EH. Solution-processed infrared photovoltaic devices with >10% monochromatic internal quantum efficiency. Appl Phys Lett 2005, 87, 213112.
[140] Johnston KW, Pattantyus-Abraham AG, Clifford JP, et al. Schottky-quantum dot photovoltaics for efficient infrared power conversion. Appl Phys Lett 2008, 92, 151115.
[141] Johnston KW, Pattantyus-Abraham AG, Clifford JP, et al. Efficient Schottky-quantum-dot photovoltaics: The roles of depletion, drift, and diffusion. Appl Phys Lett 2008, 92, 122111.
[142] Debnath R, Tang J, Barkhouse DA, et al. Ambient-Processed Colloidal Quantum Dot Solar Cells via Individual Pre-Encapsulation of Nanoparticles. J Am Chem Soc 2010, 132, 5952–3.
[143] Tang J, Wang X, Brzozowski L, et al. Schottky Quantum Dot Solar Cells Stable in Air under Solar Illumination. Adv Mater 2010, 22, 1398–402.
[144] Mai X-D, An HJ, Song JH, Jang J, Kim S, Jeong S. Inverted Schottky quantum dot solar cells with enhanced carrier ex-

traction and air-stability. J Mater Chem A 2014, 2, 20799–805.
[145] Choi M-J, Oh J, Yoo J-K, Choi J, Sim DM, Jung YS. Tailoring of the PbS/metal interface in colloidal quantum dot solar cells for improvements of performance and air stability. Energy Environ Sci 2014, 7, 3052–60.
[146] Piliego C, Protesescu L, Bisri SZ, Kovalenko MV, Loi MA. 5.2% efficient PbS nanocrystal Schottky solar cells. Energy Environ Sci 2013, 6, 3054–9.
[147] Nelson J. The physics of solar cells. 2003. London: Imperial College Press, n.d.
[148] Henry CH. Limiting efficiencies of ideal single and multiple energy gap terrestrial solar cells. J Appl Phys 1980, 51, 4494–500.
[149] Gur I, Fromer NA, Geier ML, Alivisatos AP. Air-Stable All-Inorganic Nanocrystal Solar Cells Processed from Solution. Science 2005, 310, 462–5.
[150] Greenham NC, Peng X, Alivisatos AP. Charge separation and transport in conjugated-polymer/semiconductor-nanocrystal composites studied by photoluminescence quenching and photoconductivity. Phys Rev B 1996, 54, 17628–37.
[151] Huynh WU, Dittmer JJ, Alivisatos AP. Hybrid Nanorod-Polymer Solar Cells. Science 2002, 295, 2425–7.
[152] Wehrenberg BL, Wang C, Guyot-Sionnest P. Interband and Intraband Optical Studies of PbSe Colloidal Quantum Dots. J Phys Chem B 2002, 106, 10634–40.
[153] Shim M, Guyot-Sionnest P. Permanent dipole moment and charges in colloidal semiconductor quantum dots. J Chem Phys 1999, 111, 6955–64.
[154] Blanton SA, Leheny RL, Hines MA, Guyot-Sionnest P. Dielectric Dispersion Measurements of CdSe Nanocrystal Colloids: Observation of a Permanent Dipole Moment. Phys Rev Lett 1997, 79, 865–8.
[155] Stievater TH, Li X, Steel DG, et al. Rabi Oscillations of Excitons in Single Quantum Dots. Phys Rev Lett 2001, 87, 133603.
[156] Pan Z, Zhao K, Wang J, Zhang H, Feng Y, Zhong X. Near Infrared Absorption of $CdSe_xTe_{1-x}$ Alloyed Quantum Dot Sensitized Solar Cells with More than 6% Efficiency and High Stability. ACS Nano 2013, 7, 5215–22.
[157] Santra PK, Kamat PV. Mn-Doped Quantum Dot Sensitized Solar Cells: A Strategy to Boost Efficiency over 5%. J Am Chem Soc 2012, 134, 2508–11.
[158] McElroy N, Page RC, Espinbarro-Valazquez D, et al. Comparison of solar cells sensitised by CdTe/CdSe and CdSe/CdTe core/shell colloidal quantum dots with and without a CdS outer layer. Thin Solid Films 2014, 560, 65–70.
[159] Guijarro N, Lana-Villarreal T, Mora-Seró I, Bisquert J, Gómez R. CdSe Quantum Dot-Sensitized TiO2 Electrodes: Effect of Quantum Dot Coverage and Mode of Attachment. J Phys Chem C 2009, 113, 4208–14.
[160] Chen J, Song JL, Sun XW, et al. An oleic acid-capped CdSe quantum-dot sensitized solar cell. Appl Phys Lett 2009, 94, 153115.
[161] Lee H, Wang M, Chen P, et al. Efficient CdSe Quantum Dot-Sensitized Solar Cells Prepared by an Improved Successive Ionic Layer Adsorption and Reaction Process. Nano Lett 2009, 9, 4221–7.
[162] Wijayantha KGU, Peter LM, Otley LC. Fabrication of CdS quantum dot sensitized solar cells via a pressing route. Sol Energy Mater Sol Cells 2004, 83, 363–9.
[163] Salant A, Shalom M, Hod I, Faust A, Zaban A, Banin U. Quantum Dot Sensitized Solar Cells with Improved Efficiency Prepared Using Electrophoretic Deposition. ACS Nano 2010, 4, 5962–8.
[164] Roelofs KE, Herron SM, Bent SF. Increased Quantum Dot Loading by pH Control Reduces Interfacial Recombination in Quantum-Dot-Sensitized Solar Cells. ACS Nano 2015, 9, 8321–34.
[165] Kaiser I, Ernst K, Fischer C-H, et al. The eta-solar cell with $CuInS_2$: A photovoltaic cell concept using an extremely thin absorber (eta). Sol Energy Mater Sol Cells 2001, 67, 89–96.
[166] Vogel R, Hoyer P, Weller H. Quantum-Sized PbS, CdS, Ag_2S, Sb_2S3, and Bi_2S3 Particles as Sensitizers for Various Nanoporous Wide-Bandgap Semiconductors. J Phys Chem 1994, 98, 3183–8.
[167] Hoyer P, Könenkamp R. Photoconduction in porous TiO2 sensitized by PbS quantum dots. Appl Phys Lett 1995, 66, 349–51.
[168] Liu D, Kamat PV. Photoelectrochemical behavior of thin cadmium selenide and coupled titania/cadmium selenide semiconductor films. J Phys Chem 1993, 97, 10769–73.
[169] Lee H, Leventis HC, Moon S-J, et al. PbS and CdS Quantum Dot-Sensitized Solid-State Solar Cells: "Old Concepts, New Results." Adv Funct Mater 2009, 19, 2735–42.
[170] Herzog C, Belaidi A, Ogacho A, Dittrich T. Inorganic solid state solar cell with ultra-thin nanocomposite absorber based on nanoporous TiO_2 and In_2S_3. Energy Environ Sci 2009, 2, 962–4.
[171] Krunks M, Kärber E, Katerski A, et al. Extremely thin absorber layer solar cells on zinc oxide nanorods by chemical spray. Sol Energy Mater Sol Cells 2010, 94, 1191–5.
[172] Jumabekov AN, Siegler TD, Cordes N, et al. Comparison of Solid-State Quantum-Dot-Sensitized Solar Cells with ex Situ and in Situ Grown PbS Quantum Dots. J Phys Chem C 2014, 118, 25853–62.
[173] Zhao K, Yu H, Zhang H, Zhong X. Electroplating Cuprous Sulfide Counter Electrode for High-Efficiency Long-Term Stability Quantum Dot Sensitized Solar Cells. J Phys Chem C 2014, 118, 5683–90.
[174] Jiang Y, Zhang X, Ge Q-Q, et al. ITO@Cu_2S Tunnel Junction Nanowire Arrays as Efficient Counter Electrode for Quantum-Dot-Sensitized Solar Cells. Nano Lett 2014, 14, 365–72.
[175] Chen H, Zhu L, Liu H, Li W. ITO Porous Film-Supported Metal Sulfide Counter Electrodes for High-Performance Quantum-Dot-Sensitized Solar Cells. J Phys Chem C 2013, 117, 3739–46.
[176] Yang Y, Zhu L, Sun H, et al. Composite Counter Electrode Based on Nanoparticulate PbS and Carbon Black: Towards Quantum Dot-Sensitized Solar Cells with Both High Efficiency and Stability. ACS Appl Mater Interfaces 2012, 4, 6162–8.
[177] Wang J, Mora-Seró I, Pan Z, et al. Core/Shell Colloidal Quantum Dot Exciplex States for the Development of Highly Efficient Quantum-Dot-Sensitized Solar Cells. J Am Chem Soc 2013, 135, 15913–22.
[178] Pan Z, Mora-Seró I, Shen Q, et al. High-Efficiency "Green" Quantum Dot Solar Cells. J Am Chem Soc 2014, 136, 9203–10.
[179] Li L, Yang X, Gao J, et al. Highly Efficient CdS Quantum Dot-Sensitized Solar Cells Based on a Modified Polysulfide Electrolyte. J Am Chem Soc 2011, 133, 8458–60.

[180] Zhao K, Pan Z, Mora-Seró I, et al. Boosting Power Conversion Efficiencies of Quantum-Dot-Sensitized Solar Cells Beyond 8% by Recombination Control. J Am Chem Soc 2015, 137, 5602–9.
[181] Pattantyus-Abraham AG, Kramer IJ, Barkhouse AR, et al. Depleted-Heterojunction Colloidal Quantum Dot Solar Cells. ACS Nano 2010, 4, 3374–80.
[182] Willis SM, Cheng C, Assender HE, Watt AAR. The Transitional Heterojunction Behavior of PbS/ZnO Colloidal Quantum Dot Solar Cells. Nano Lett 2012, 12, 1522–6.
[183] Ko D-K, Brown PR, Bawendi MG, Bulović V. p-i-n Heterojunction Solar Cells with a Colloidal Quantum-Dot Absorber Layer. Adv Mater 2014, 26, 4845–50.
[184] Gao J, Luther JM, Semonin OE, Ellingson RJ, Nozik AJ, Beard MC. Quantum Dot Size Dependent J–V Characteristics in Heterojunction ZnO/PbS Quantum Dot Solar Cells. Nano Lett 2011, 11, 1002–8.
[185] Schnitzenbaumer KJ, Labrador T, Dukovic G. Impact of Chalcogenide Ligands on Excited State Dynamics in CdSe Quantum Dots. J Phys Chem C 2015, 119, 13314–24.
[186] Cademartiri L, Montanari E, Calestani G, Migliori A, Guagliardi A, Ozin GA. Size-Dependent Extinction Coefficients of PbS Quantum Dots. J Am Chem Soc 2006, 128, 10337–46.
[187] Yoon W, Boercker JE, Lumb MP, Placencia D, Foos EE, Tischler JG. Enhanced Open-Circuit Voltage of PbS Nanocrystal Quantum Dot Solar Cells. Sci Rep 2013, 3.
[188] Sun Z, Sitbon G, Pons T, Bakulin AA, Chen Z. Reduced Carrier Recombination in PbS - $CuInS_2$ Quantum Dot Solar Cells. Sci Rep 2015, 5.
[189] Park SH, Roy A, Beaupré S, et al. Bulk heterojunction solar cells with internal quantum efficiency approaching 100%. Nat Photonics 2009, 3, 297–302.
[190] Liang Y, Feng D, Wu Y, et al. Highly Efficient Solar Cell Polymers Developed via Fine-Tuning of Structural and Electronic Properties. J Am Chem Soc 2009, 131, 7792–9.
[191] Lee MM, Teuscher J, Miyasaka T, Murakami TN, Snaith HJ. Efficient Hybrid Solar Cells Based on Meso-Superstructured Organometal Halide Perovskites. Science 2012, 338, 643–7.
[192] Heremans P, Cheyns D, Rand BP. Strategies for Increasing the Efficiency of Heterojunction Organic Solar Cells: Material Selection and Device Architecture. Acc Chem Res 2009, 42, 1740–7.
[193] Kim JY, Kim SH, Lee H-H, et al. New Architecture for High-Efficiency Polymer Photovoltaic Cells Using Solution-Based Titanium Oxide as an Optical Spacer. Adv Mater 2006, 18, 572–6.
[194] Kramer IJ, Sargent EH. The Architecture of Colloidal Quantum Dot Solar Cells: Materials to Devices. Chem Rev 2014, 114, 863–82.
[195] Im J-H, Lee C-R, Lee J-W, Park S-W, Park N-G. 6.5% efficient perovskite quantum-dot-sensitized solar cell. Nanoscale 2011, 3, 4088–93.
[196] Heo JH, Im SH, Noh JH, et al. Efficient inorganic-organic hybrid heterojunction solar cells containing perovskite compound and polymeric hole conductors. Nat Photonics 2013, 7, 486–91.
[197] Dabirian A, Taghavinia N. Theoretical Study of Light Trapping in Nanostructured Thin Film Solar Cells Using Wavelength-Scale Silver Particles. ACS Appl Mater Interfaces 2015.
[198] Niggemann M, Riede M, Gombert A, Leo K. Light trapping in organic solar cells. Phys Status Solidi A 2008, 205, 2862–74.
[199] Rim S-B, Zhao S, Scully SR, McGehee MD, Peumans P. An effective light trapping configuration for thin-film solar cells. Appl Phys Lett 2007, 91, 243501.
[200] Polman A, Atwater HA. Photonic design principles for ultrahigh-efficiency photovoltaics. Nat Mater 2012, 11, 174–7.
[201] Chou C-H, Chen F-C. Plasmonic nanostructures for light trapping in organic photovoltaic devices. Nanoscale 2014, 6, 8444.
[202] Zhang W, Saliba M, Stranks SD, et al. Enhancement of Perovskite-Based Solar Cells Employing Core–Shell Metal Nanoparticles. Nano Lett 2013, 13, 4505–10.
[203] Atwater HA. The Promise of Plasmonics. Sci Am 2007, 296, 56–62.
[204] Gramotnev DK, Bozhevolnyi SI. Plasmonics beyond the diffraction limit. Nat Photonics 2010, 4, 83–91.
[205] Schuller JA, Barnard ES, Cai W, Jun YC, White JS, Brongersma ML. Plasmonics for extreme light concentration and manipulation. Nat Mater 2010, 9, 193–204.
[206] Maier SA, Atwater HA. Plasmonics: Localization and guiding of electromagnetic energy in metal/dielectric structures. J Appl Phys 2005, 98, 011101.
[207] Ozbay E. Plasmonics: Merging Photonics and Electronics at Nanoscale Dimensions. Science 2006, 311, 189–93.
[208] Maier SA. Plasmonics: Fundamentals and Applications. Springer Science & Business Media, 2007.
[209] Lan X, Bai J, Masala S, et al. Self-Assembled, Nanowire Network Electrodes for Depleted Bulk Heterojunction Solar Cells. Adv Mater 2013, 25, 1769–73.
[210] Kramer IJ, Zhitomirsky D, Bass JD, et al. Ordered Nanopillar Structured Electrodes for Depleted Bulk Heterojunction Colloidal Quantum Dot Solar Cells. Adv Mater 2012, 24, 2315–9.
[211] Jean J, Chang S, Brown PR, et al. ZnO Nanowire Arrays for Enhanced Photocurrent in PbS Quantum Dot Solar Cells. Adv Mater 2013, 25, 2790–6.
[212] Rath AK, Bernechea M, Martinez L, de Arquer FPG, Osmond J, Konstantatos G. Solution-processed inorganic bulk nanoheterojunctions and their application to solar cells. Nat Photonics 2012, 6, 529–34.
[213] Tan F, Qu S, Jiang Q, et al. Interpenetrated Inorganic Hybrids for Efficiency Enhancement of PbS Quantum Dot Solar Cells. Adv Energy Mater 2014, 4, n/a – n/a.
[214] Etgar L, Yanover D, Čapek RK, et al. Core/Shell PbSe/PbS QDs TiO2 Heterojunction Solar Cell. Adv Funct Mater 2013, 23, 2736–41.
[215] Ning Z, Zhitomirsky D, Adinolfi V, et al. Graded Doping for Enhanced Colloidal Quantum Dot Photovoltaics. Adv Mater 2013, 25, 1719–23.
[216] Yuan M, Zhitomirsky D, Adinolfi V, et al. Doping Control Via Molecularly Engineered Surface Ligand Coordination. Adv Mater 2013, 25, 5586–92.
[217] Hoye RLZ, Ehrler B, Böhm ML, et al. Improved Open- Circuit Voltage in ZnO–PbSe Quantum Dot Solar Cells by Understanding and Reducing Losses Arising from the ZnO Conduction Band Tail. Adv Energy Mater 2014, 4, n/a – n/a.
[218] Chang J, Kuga Y, Mora-Seró I, et al. High reduction of interfacial charge recombination in colloidal quantum dot solar cells by metal oxide surface passivation. Nanoscale 2015, 7, 5446–56.

[219] Kim JY, Voznyy O, Zhitomirsky D, Sargent EH. 25th Anniversary Article: Colloidal Quantum Dot Materials and Devices: A Quarter-Century of Advances. Adv Mater 2013, 25, 4986–5010.
[220] Yuan M, Voznyy O, Zhitomirsky D, Kanjanaboos P, Sargent EH. Synergistic Doping of Fullerene Electron Transport Layer and Colloidal Quantum Dot Solids Enhances Solar Cell Performance. Adv Mater 2015, 27, 917–21.
[221] Nam M, Park J, Lee K, et al. A multifunctional fullerene interlayer in colloidal quantum dot-based hybrid solar cells. J Mater Chem A 2015, 3, 10585–91.
[222] Shi J, Zhao P, Wang X. Piezoelectric-Polarization-Enhanced Photovoltaic Performance in Depleted-Heterojunction Quantum-Dot Solar Cells. Adv Mater 2013, 25, 916–21.
[223] Brown PR, Lunt RR, Zhao N, et al. Improved Current Extraction from ZnO/PbS Quantum Dot Heterojunction Photovoltaics Using a MoO3 Interfacial Layer. Nano Lett 2011, 11, 2955–61.
[224] Brown PR, Kim D, Lunt RR, et al. Energy Level Modification in Lead Sulfide Quantum Dot Thin Films through Ligand Exchange. ACS Nano 2014, 8, 5863–72.
[225] Gonfa BA, Kim MR, Delegan N, et al. Towards high efficiency air-processed near-infrared responsive photovoltaics: bulk heterojunction solar cells based on PbS/CdS core–shell quantum dots and TiO2 nanorod arrays. Nanoscale 2015, 7, 10039–49.
[226] Xu F, Ma X, Haughn CR, Benavides J, Doty MF, Cloutier SG. Efficient Exciton Funneling in Cascaded PbS Quantum Dot Superstructures. ACS Nano 2011, 5, 9950–7.
[227] Kim JY, Adinolfi V, Sutherland BR, et al. Single-step fabrication of quantum funnels via centrifugal colloidal casting of nanoparticle films. Nat Commun 2015, 6.
[228] Voznyy O, Zhitomirsky D, Stadler P, Ning Z, Hoogland S, Sargent EH. A Charge-Orbital Balance Picture of Doping in Colloidal Quantum Dot Solids. ACS Nano 2012, 6, 8448–55.
[229] Liu H, Zhitomirsky D, Hoogland S, et al. Systematic optimization of quantum junction colloidal quantum dot solar cells. Appl Phys Lett 2012, 101, 151112.
[230] Stavrinadis A, Rath AK, de Arquer FPG, et al. Heterovalent cation substitutional doping for quantum dot homojunction solar cells. Nat Commun 2013, 4.
[231] Adinolfi V., Ning Z., Xu J., et al. Electric field engineering using quantum-size-effect-tuned heterojunctions. Appl Phys Lett 2013, 103, 011106–011106 – 4.
[232] Cheng C, Lee MM, Noel NK, et al. Polystyrene Templated Porous Titania Wells for Quantum Dot Heterojunction Solar Cells. ACS Appl Mater Interfaces 2014, 6, 14247–52.
[233] Labelle AJ, Thon SM, Masala S, et al. Colloidal Quantum Dot Solar Cells Exploiting Hierarchical Structuring. Nano Lett 2015, 15, 1101–8.
[234] Mihi A, Beck FJ, Lasanta T, Rath AK, Konstantatos G. Imprinted Electrodes for Enhanced Light Trapping in Solution Processed Solar Cells. Adv Mater 2014, 26, 443–8.
[235] Adachi MM, Labelle AJ, Thon SM, Lan X, Hoogland S, Sargent EH. Broadband solar absorption enhancement via periodic nanostructuring of electrodes. Sci Rep 2013, 3.
[236] Koleilat GI, Kramer IJ, Wong CTO, et al. Folded-Light-Path Colloidal Quantum Dot Solar Cells. Sci Rep 2013, 3.
[237] Kim G-H, Walker B, Kim H-B, et al. Inverted Colloidal Quantum Dot Solar Cells. Adv Mater 2014, 26, 3321–7.
[238] Atwater HA, Polman A. Plasmonics for improved photovoltaic devices. Nat Mater 2010, 9, 205–13.
[239] Green MA, Pillai S. Harnessing plasmonics for solar cells. Nat Photonics 2012, 6, 130–2.
[240] Paz-Soldan D, Lee A, Thon SM, et al. Jointly Tuned Plasmonic–Excitonic Photovoltaics Using Nanoshells. Nano Lett 2013, 13, 1502–8.
[241] Kawawaki T, Wang H, Kubo T, et al. Efficiency Enhancement of PbS Quantum Dot/ZnO Nanowire Bulk-Heterojunction Solar Cells by Plasmonic Silver Nanocubes. ACS Nano 2015, 9, 4165–72.
[242] Yablonovitch E. Statistical ray optics. J Opt Soc Am 1982, 72, 899.
[243] Kholmicheva N, Moroz P, Rijal U, et al. Plasmonic Nanocrystal Solar Cells Utilizing Strongly Confined Radiation. ACS Nano 2014, 8, 12549–59.
[244] Beck FJ, Stavrinadis A, Diedenhofen SL, Lasanta T, Konstantatos G. Surface Plasmon Polariton Couplers for Light Trapping in Thin-Film Absorbers and Their Application to Colloidal Quantum Dot Optoelectronics. ACS Photonics 2014, 1, 1197–205.
[245] Beck FJ, Lasanta T, Konstantatos G. Plasmonic Schottky Nanojunctions for Tailoring the Photogeneration Profile in Thin Film Solar Cells. Adv Opt Mater 2014, 2, 493–500.
[246] Cotal H, Fetzer C, Boisvert J, et al. III–V multijunction solar cells for concentrating photovoltaics. Energy Environ Sci 2009, 2, 174–92.
[247] Chen C-C, Chang W-H, Yoshimura K, et al. An Efficient Triple-Junction Polymer Solar Cell Having a Power Conversion Efficiency Exceeding 11%. Adv Mater 2014, 26, 5670–7.
[248] Koleilat GI, Wang X, Sargent EH. Graded Recombination Layers for Multijunction Photovoltaics. Nano Lett 2012, 12, 3043–9.
[249] Speirs MJ, Groeneveld BGHM, Protesescu L, Piliego C, Kovalenko MV, Loi MA. Hybrid inorganic–organic tandem solar cells for broad absorption of the solar spectrum. Phys Chem Chem Phys 2014, 16, 7672–6.
[250] Koleilat GI, Wang X, Labelle AJ, et al. A Donor-Supply Electrode (DSE) for Colloidal Quantum Dot Photovoltaics. Nano Lett 2011, 11, 5173–8.
[251] Ma W, Luther JM, Zheng H, Wu Y, Alivisatos AP. Photovoltaic Devices Employing Ternary PbSxSe1-x Nanocrystals. Nano Lett 2009, 9, 1699–703.
[252] Ip AH, Kiani A, Kramer IJ, et al. Infrared Colloidal Quantum Dot Photovoltaics via Coupling Enhancement and Agglomeration Suppression. ACS Nano 2015, 9, 8833–42.
[253] Zhu H, Lian T. Enhanced Multiple Exciton Dissociation from CdSe Quantum Rods: The Effect of Nanocrystal Shape. J Am Chem Soc 2012, 134, 11289–97.
[254] Stolle CJ, Harvey TB, Pernik DR, et al. Multiexciton Solar Cells of CuInSe2 Nanocrystals. J Phys Chem Lett 2014, 5, 304–9.
[255] Stolle CJ, Schaller RD, Korgel BA. Efficient Carrier Multiplication in Colloidal CuInSe2 Nanocrystals. J Phys Chem Lett 2014, 5, 3169–74.
[256] Semonin OE, Luther JM, Choi S, et al. Peak External Photocurrent Quantum Efficiency Exceeding 100% via MEG in a Quantum Dot Solar Cell. Science 2011, 334, 1530–3.
[257] Midgett AG, Luther JM, Stewart JT, et al. Size and Composition Dependent Multiple Exciton Generation Efficiency in

PbS, PbSe, and PbSxSe1–x Alloyed Quantum Dots. Nano Lett 2013, 13, 3078–85.
[258] Marshall AR, Beard MC, Luther JM. Multiple exciton generation solar cells: Effects of nanocrystal shape on quantum efficiency. Photovolt. Spec. Conf. PVSC 2014 IEEE 40th, 2014, p. 1077–9.
[259] Ono M, Nishihara T, Ihara T, et al. Impact of surface ligands on the photocurrent enhancement due to multiple exciton generation in close-packed nanocrystal thin films. Chem Sci 2014, 5, 2696–701.
[260] Geiregat P, Delerue C, Justo Y, et al. A Phonon Scattering Bottleneck for Carrier Cooling in Lead Chalcogenide Nanocrystals. ACS Nano 2015, 9, 778–88.
[261] Cirloganu CM, Padilha LA, Lin Q, et al. Enhanced carrier multiplication in engineered quasi-type-II quantum dots. Nat Commun 2014, 5.
[262] Tabachnyk M, Ehrler B, Gélinas S, et al. Resonant energy transfer of triplet excitons from pentacene to PbSe nanocrystals. Nat Mater 2014, 13, 1033–8.
[263] Thompson NJ, Wilson MWB, Congreve DN, et al. Energy harvesting of non-emissive triplet excitons in tetracene by emissive PbS nanocrystals. Nat Mater 2014, 13, 1039–43.
[264] Shcherbatyuk GV, Inman RH, Wang C, Winston R, Ghosh S. Viability of using near infrared PbS quantum dots as active materials in luminescent solar concentrators. Appl Phys Lett 2010, 96, 191901.
[265] Viswanatha R, Brovelli S, Pandey A, Crooker SA, Klimov VI. Copper-Doped Inverted Core/Shell Nanocrystals with "Permanent" Optically Active Holes. Nano Lett 2011, 11, 4753–8.
[266] Meinardi F, Colombo A, Velizhanin KA, et al. Large-area luminescent solar concentrators based on /'Stokes-shift-engineered/' nanocrystals in a mass-polymerized PMMA matrix. Nat Photonics 2014, 8, 392–9.
[267] Coropceanu I, Bawendi MG. Core/Shell Quantum Dot Based Luminescent Solar Concentrators with Reduced Reabsorption and Enhanced Efficiency. Nano Lett 2014, 14, 4097–101.
[268] Erickson CS, Bradshaw LR, McDowall S, Gilbertson JD, Gamelin DR, Patrick DL. Zero-Reabsorption Doped-Nanocrystal Luminescent Solar Concentrators. ACS Nano 2014, 8, 3461–7.
[269] Bradshaw LR, Knowles KE, McDowall S, Gamelin DR. Nanocrystals for Luminescent Solar Concentrators. Nano Lett 2015, 15, 1315–23.
[270] Meinardi F, McDaniel H, Carulli F, et al. Highly efficient large-area colourless luminescent solar concentrators using heavy-metal-free colloidal quantum dots. Nat Nanotechnol 2015, 10, 878–85.
[271] Bronstein ND, Yao Y, Xu L, et al. Quantum Dot Luminescent Concentrator Cavity Exhibiting 30-fold Concentration. ACS Photonics 2015.
[272] Zhitomirsky D, Voznyy O, Levina L, et al. Engineering colloidal quantum dot solids within and beyond the mobility-invariant regime. Nat Commun 2014, 5.
[273] Ning Z, Gong X, Comin R, et al. Quantum-dot-in-perovskite solids. Nature 2015, 523, 324–8.